Journal of
Polymer Materials

Tech Science Press

https://doi.org/10.32604/jpm.2026.080437

ARTICLE

Application of a Waste Cotton–Based Graft-Modified Polymer in Shale Gas Water-Based Drilling Fluids: Rheological Regulation, Filtration Control, and Mechanism

Feng Dai[1], Jiajun Xie[1], Yingmin Liu[1], De Heng[1], Yinfu Han[2,3] and Shanshan Hou[2,3,*]

[1]Sichuan Changning Gas Development Co., Ltd., Changning, China
[2]Collaborative Innovation Center for Unconventional Oil and Gas, Yangtze University, Wuhan, China
[3]Hubei Engineering Research Centers for Clean Production and Pollution Control of Oil and Gas Fields, Jingzhou, China

*Corresponding Author: Shanshan Hou. Email: hss250606@163.com

Received: 09 February 2026; Accepted: 12 May 2026; Published: 30 June 2026

ABSTRACT: With the increasing emphasis on green, low-carbon, and sustainable development in shale gas drilling fluids, the utilization of waste biomass resources to develop high-performance drilling fluid additives has emerged as an important research direction that balances engineering requirements with environmental responsibility. In this study, waste cotton–derived polyanionic cellulose (bio-PAC) was employed as the base material, and sulfonate and carboxylate functional groups were introduced via free-radical graft copolymerization to synthesize a modified cellulose polymer, PAC-g-(sodium vinyl sulfonate, SVS/sodium methallyl sulfonate, SMAS/methacrylic acid, MAA). Structural characterization confirmed the successful grafting of the target functional groups onto the cellulose backbone. The resulting polymer exhibited high thermal stability, with a decomposition temperature up to 330°C under a nitrogen atmosphere, and demonstrated favorable environmental compatibility (EC_{50} = 73,000 mg/L). Performance evaluation showed that, in bentonite-based mud systems, the addition of 30 g/L PAC-g-(SVS/SMAS/MAA) followed by aging at 160°C for 16 h resulted in apparent viscosity (AV) retention rates of 81.3%, 73.6%, and 76.4% in freshwater, saturated brine, and mixed-salt based muds, respectively, while the corresponding low-temperature low-pressure (LTLP) filtration volumes were all below 5.0 mL. In shale gas water-based drilling fluid systems, when the dosage was 20 g/L, the drilling fluids maintained stable rheological structures after high-temperature aging at 160°C–180°C, with AV values of 33.5–42.5 mPa·s and yield point (YP) values exceeding 8.5 Pa, significantly outperforming commercial hydroxyethyl cellulose (HEC)– and polyanionic cellulose (PAC)–treated systems. Meanwhile, the high-temperature high-pressure (HTHP) filtration volumes were reduced to 9.8–18.6 mL, corresponding to reduction rates of 82.2%–91.3%. Scanning electron microscopy (SEM) observations of the filter cakes revealed that PAC-g-(SVS/SMAS/MAA) promoted the formation of continuous and compact filtration barrier structures under high-temperature conditions, thereby effectively inhibiting particle migration and pore connectivity. These results demonstrate that the developed polymer can simultaneously achieve significant viscosity enhancement and efficient filtration control in high-temperature shale gas water-based drilling fluids, indicating promising potential for practical engineering applications.

KEYWORDS: Shale gas water-based drilling fluids; cellulose derivatives; graft copolymerization; thermal and salt resistance; rheological regulation and filtration control

1 Introduction

With the continuous large-scale development of unconventional oil and gas resources, particularly shale gas, drilling operations are progressively extending toward high-temperature, high-salinity, and geologically

complex formations, thereby imposing increasingly stringent requirements on the overall performance of water-based drilling fluids [1–4]. Drilling fluids are required not only to provide effective rheological regulation to ensure adequate hole cleaning and cuttings transport, but also to form dense and stable filter cakes under high-temperature and high-pressure conditions, so as to control fluid loss and protect the formation [5,6]. Compared with oil-based drilling fluids, water-based drilling fluids offer advantages in terms of environmental compatibility and cost effectiveness [7]. However, under high-temperature and high-mineralization conditions, water-based drilling fluid systems often suffer from severe degradation of rheological structures and a sharp increase in filtration loss, which substantially limits their engineering performance and field applicability [8,9].

Modified cellulose-based polymers have long been employed as key additives in water-based drilling fluids owing to their favorable viscosity-enhancing capability, effective fluid-loss control performance, and environmental friendliness [10–12]. Among them, carboxymethyl cellulose (CMC), polyanionic cellulose (PAC), and hydroxyethyl cellulose (HEC) have been extensively applied in field operations [13,14]. In addition, cellulose nanomaterials, such as cellulose nanofibers (CNFs) and cellulose nanocrystals (CNCs), have attracted increasing attention in the regulation of rheological properties and fluid-loss control of drilling fluids due to their high specific surface area, strong hydration capability, and nanoscale structural features [13,15,16]. For example, Khan et al. [17] reported that mechanically disintegrated CNFs (M-CNFs), characterized by highly entangled network structures, contribute to the enhancement of rheological properties, whereas TEMPO-mediated oxidized CNFs (T-CNFs), possessing a higher density of surface negative charges, can suppress bentonite flocculation by enhancing interparticle electrostatic repulsion, thereby contributing to fluid-loss control.

However, both conventional cellulose derivatives and unmodified cellulose nanomaterial systems still face significant challenges under high-temperature and high-salinity conditions [18,19]. On the one hand, the side-chain structures of these materials are predominantly composed of nonionic or weakly ionizable functional groups. In highly mineralized environments, the presence of large amounts of electrolytes compresses the electrical double layer surrounding the polymer chains, weakens electrostatic repulsion between chain segments, and induces chain coiling or even conformational collapse [20,21]. On the other hand, elevated temperatures markedly intensify the thermal motion of polymer chains, leading to reduced stability of the adsorption layers on solid surfaces and a higher tendency toward desorption or molecular rearrangement. This, in turn, diminishes interparticle bridging interactions and weakens the overall structural strength of the fluid system [22]. As a result, conventional modified cellulose polymers often suffer from severe deterioration of rheological parameters, loose filter cake structures, and uncontrolled filtration loss in high-temperature, high-salinity drilling fluid systems, rendering them inadequate for the engineering requirements of deep and ultra-deep shale gas wells.

In recent years, the introduction of strongly hydrophilic ionic functional groups onto cellulose backbones via chemical grafting or copolymerization has been widely regarded as an effective approach to enhancing thermal and salt tolerance [23]. In particular, sulfonate groups, owing to their strong ionization capability and robust hydration characteristics even under high-salinity conditions, contribute to maintaining extended polymer chain conformations and improving solution structural stability [24–26]. Nevertheless, most existing studies have focused primarily on the enhancement of single performance attributes, making it difficult to achieve synergistic optimization between viscosity enhancement and filtration reduction. Moreover, a systematic understanding of the underlying mechanisms governing their behavior in complex drilling fluid systems remains insufficient. In this context, sodium vinyl sulfonate (SVS), sodium methallyl sulfonate (SMAS), and a small amount of methacrylic acid (MAA) were selected as grafting monomers in this study. SVS, characterized by its simple structure, high reactivity, and strong

anionic nature, can introduce a high density of sulfonate sites onto the cellulose backbone, thereby enhancing hydrophilicity, ionization stability, and interchain electrostatic repulsion. This contributes to mitigating polymer coil contraction induced by electrical double-layer compression under high-salinity conditions and helps maintain an extended chain conformation [27,28]. SMAS, containing a methyl substituent, provides steric hindrance that can regulate side-chain conformation and improve thermal stability, while retaining the hydration and salt-resistance characteristics of sulfonate groups [28,29]. In addition, the incorporation of a limited amount of MAA introduces carboxylate functionalities, which facilitate adsorption and bridging interactions between the polymer and bentonite or other solid particles, thereby promoting particle aggregation and pore filling and contributing to improved filtration control [30]. However, in systems containing multivalent cations such as Ca^{2+} and Mg^{2+}, excessive carboxylate content may induce unfavorable ionic bridging effects [31]. Therefore, only a small amount of MAA was introduced to achieve a balance between adsorption enhancement and salt tolerance. Based on this design, the combined incorporation of SVS, SMAS, and a limited amount of MAA aims to simultaneously enhance hydration stability in the bulk solution and adsorption regulation at solid interfaces, thereby enabling synergistic optimization of rheological regulation and filtration control.

From the perspective of raw material selection, textile wastes such as waste cotton represent a high-purity cellulose biomass resource characterized by high cellulose content (95%–99%), low impurity levels, and stable availability, making them ideal precursors for the preparation of high-performance cellulose derivatives [32,33]. In contrast to lignocellulosic materials, waste cotton contains negligible amounts of lignin and hemicellulose, thereby avoiding complex removal processes and facilitating the acquisition of cellulose substrates with more uniform structures and higher chemical reactivity [34,35]. Moreover, the high-value utilization of discarded cotton fibers is consistent with the ongoing trend toward greener oilfield chemical technologies. Accordingly, the development of environmentally friendly, high-performance drilling fluid additives based on waste cotton is of both engineering significance and environmental relevance.

Based on these considerations, a novel graft-modified polymer, PAC-g-(SVS/SMAS/MAA), was synthesized via free-radical graft copolymerization using waste cotton–derived bio-PAC as the base material. The effects of synthesis conditions on material properties were systematically investigated, and the thermal resistance, salt tolerance, rheological regulation, and filtration control performance of the resulting polymer were comprehensively evaluated in bentonite-based mud and shale gas water-based drilling fluid systems. Furthermore, the underlying mechanisms governing its performance under high-temperature conditions were elucidated through a combination of rheological measurements, filtration tests, and microstructural characterization of filter cakes. The findings of this work are expected to provide useful insights for the design and application of high-performance, environmentally friendly cellulose-based additives for high-temperature shale gas water-based drilling fluids.

2 Materials and Methods

A schematic overview of the research workflow is presented in Fig. 1, including synthesis optimization, material characterization, performance evaluation, and mechanism analysis of PAC-g-(SVS/SMAS/MAA) in shale gas water-based drilling fluids.

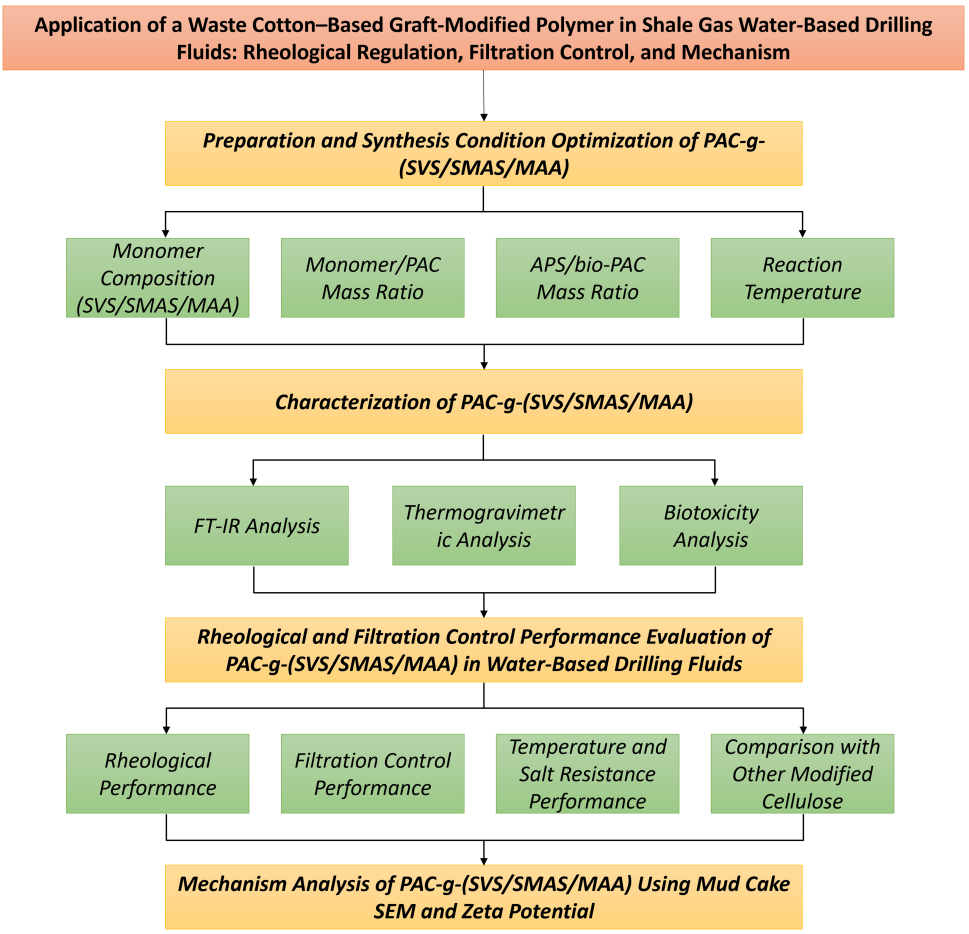

Figure 1: Schematic illustration of the overall workflow of this study.

2.1 Materials

Waste cotton fibers were obtained from discarded pure cotton textiles (self-provided) and used as the cellulose raw material for the preparation of the modified polymer after appropriate pretreatment. Sodium vinyl sulfonate (SVS), sodium methallyl sulfonate (SMAS), methacrylic acid (MAA), and ammonium persulfate (APS) were all of analytical grade and purchased from Shanghai Aladdin Biochemical Technology Co., Ltd., and were used for the graft copolymerization reactions. Sodium hydroxide, isopropanol, ethanol, glacial acetic acid, sodium chloroacetate, and hydrogen peroxide were of analytical grade and obtained from Shanghai Macklin Biochemical Co., Ltd.; all chemicals were used as received without further purification.

Sodium bentonite (meeting API specifications) was supplied by Weifang Huawei Bentonite Group Co., Ltd. (Weifang, China) and used for the preparation of bentonite-based muds and drilling fluid systems. Sodium carbonate (Na_2CO_3), sodium chloride (NaCl), calcium chloride ($CaCl_2$), and magnesium chloride hexahydrate ($MgCl_2{\cdot}6H_2O$) were of analytical grade and purchased from Shanghai Macklin Biochemical Co., Ltd., and were employed to formulate freshwater-, saturated brine-, and mixed-salt–based mud systems with different salinities. In the shale gas water-based drilling fluid formulations, inhibitors, lubricants, plugging agents, and other functional additives were supplied by Jingzhou Jiahua Technology Co., Ltd. and added according to a predefined formulation. Commercial hydroxyethyl cellulose (HEC) and commercial polyanionic cellulose (PAC) were purchased from Feicheng Yutian Chemical Co., Ltd. Deionized water was used in all experiments.

2.2 Preparation of PAC-g-(SVS/SMAS/MAA) Graft Copolymer

Biomass-derived polyanionic cellulose (bio-PAC) was prepared from waste cotton textile scraps and subsequently graft-modified to obtain the PAC-g-(SVS/SMAS/MAA) copolymer. The waste cotton was cut into small pieces (5–10 mm), thoroughly washed with deionized water, and then treated in a 1.5 wt.% nonionic surfactant solution at 60°C under stirring for 60 min to remove oils and impurities. After filtration, the fibers were rinsed with deionized water until the filtrate became clear. The cleaned cotton was then subjected to alkaline cooking in a 3.0 wt.% NaOH solution at 80°C for 1 h, followed by washing to neutrality. To further reduce color, the resulting material was treated in a 2.0 wt.% H_2O_2 alkaline solution (pH adjusted to 10.5 with NaOH) at 60°C for 1 h. The product was washed to neutrality and dried at 60°C to constant weight, yielding cellulose (bio-CEL).

For the preparation of bio-PAC, 20.0 g of bio-CEL was dispersed in 1 L of an isopropanol/water mixed medium (volume ratio 80/20) and stirred at room temperature for 15 min. A certain amount of 30 wt.% NaOH solution was then added, and the mixture was alkalized at 25°C for 60 min to form alkali cellulose. Subsequently, the temperature was raised to 55°C, and sodium chloroacetate (21.6 g) was added in three portions. The carboxymethylation reaction was carried out at 60°C for 3 h. After completion, the reaction mixture was cooled to room temperature and slowly neutralized with glacial acetic acid to pH 7.0–8.0. The slurry was poured into three times its volume of absolute ethanol to precipitate the product. The precipitate was collected by vacuum filtration and washed three times with 80% ethanol to remove byproduct salts and residual alkali. The final product was vacuum-dried at 50°C to constant weight, ground, and sieved through a 100-mesh screen to obtain polyanionic cellulose (bio-PAC) powder, with a degree of substitution of approximately 1.05.

The PAC-g-(SVS/SMAS/MAA) graft copolymer was subsequently synthesized using bio-PAC as the backbone via aqueous free-radical graft copolymerization. Briefly, 8.0 g of bio-PAC was dispersed in 792 mL of deionized water under mechanical stirring at room temperature for 30 min, followed by heating to 45°C and continued stirring for 60 min to ensure complete hydration. The system was then purged with nitrogen for 30 min to remove dissolved oxygen and maintained under a nitrogen atmosphere throughout the reaction. Monomer solutions of SVS, SMAS, and MAA were prepared at predetermined molar ratios, with MAA being pre-neutralized with NaOH to pH 7.5–8.5. After the bio-PAC solution was heated to 60°C, a certain amount of APS (30% of the total initiator dosage) was added, and the mixture was stirred for 10 min. The monomer solution was then added dropwise over 90 min, during which the remaining APS was supplemented in two portions to maintain a stable radical concentration. Upon completion of monomer addition, the reaction was allowed to proceed at 60°C for an additional 2.5 h. The reaction mixture was subsequently cooled to below 40°C and poured into three times its volume of absolute ethanol to precipitate the product. The solid was collected by vacuum filtration, washed three times with ethanol to remove free copolymers and residual salts, and finally vacuum-dried at 50°C to constant weight. The dried product was ground and sieved through a 100-mesh screen to obtain the PAC-g-(SVS/SMAS/MAA) graft copolymer powder, and its schematic molecular structure is shown in Fig. 2.

In this study, the molar ratio of SVS/SMAS/MAA, the mass ratio of total monomers to bio-PAC, the initiator dosage, and the reaction temperature were systematically varied to obtain graft copolymers with viscosity-enhancing and filtration-reducing performance suitable for drilling fluid applications.

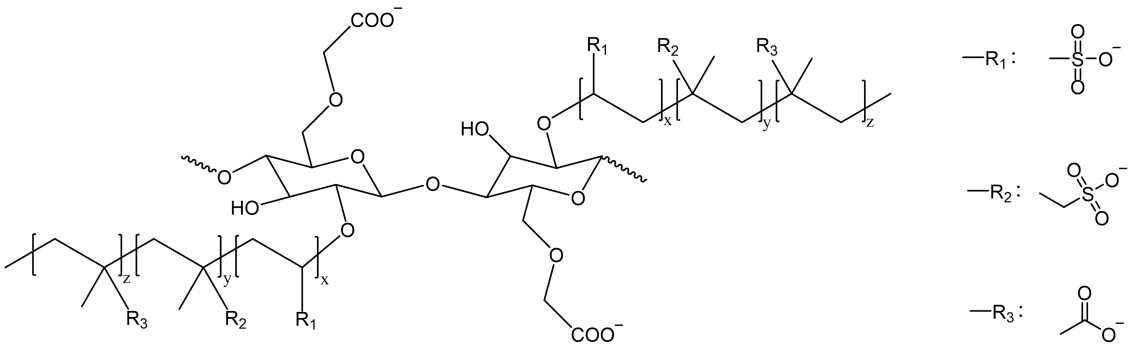

Figure 2: Schematic molecular structure of PAC-g-(SVS/SMAS/MAA).

2.3 Characterization of the Prepared Samples

Fourier transform infrared (FT-IR) spectroscopy was employed to characterize the molecular structure of the prepared PAC-g-(SVS/SMAS/MAA) samples. The polymer was thoroughly mixed with dried potassium bromide (KBr) at a mass ratio of 1:100 and compressed into transparent pellets. FT-IR spectra were recorded using a Nicolet X700 Fourier transform infrared spectrometer (Thermo Fisher Scientific, USA) over the wavenumber range of 4000–500 cm^{-1}, with a spectral resolution of 4 cm^{-1} and 32 scans accumulated for each sample.

The thermal stability of the materials was evaluated by thermogravimetric analysis (TGA) using a TGA 2 thermal analysis system (Mettler Toledo, Switzerland). Measurements were conducted under a nitrogen atmosphere with a flow rate of 50 mL/min. The samples were heated from room temperature to 600°C at a constant heating rate of 10°C/min.

To assess the potential environmental impact of the synthesized samples, their biotoxicity was evaluated using the luminescent bacteria assay, which is a widely applied rapid method for biological toxicity assessment [36]. The experimental procedures and toxicity classification were based on the half-maximal effective concentration (EC_{50}) as the evaluation criterion, and the relevant testing protocols and assessment standards were conducted in accordance with the Chinese national standard GB/T 15441-1995 [37,38].

2.4 Preparation of Bentonite-Based Muds and Shale Gas Water-Based Drilling Fluids

2.4.1 Preparation of Bentonite-Based Muds

Freshwater-based mud: A total of 400 mL of deionized water was measured, into which 1.20 g of Na_2CO_3 and 20.00 g of sodium bentonite were sequentially added. The mixture was subjected to high-speed stirring for 30 min and then aged at room temperature for 24 h to obtain the freshwater-based mud.

Saturated brine–based mud: A total of 400 mL of deionized water was taken, and 144.00 g of NaCl and 2.40 g of Na_2CO_3 were sequentially added, followed by high-speed stirring for 10 min. Subsequently, 40.00 g of sodium bentonite was added, and the mixture was further stirred at high speed for 30 min. The resulting slurry was aged at room temperature for 24 h to obtain the saturated brine–based mud.

Mixed-salt–based mud: A total of 400 mL of deionized water was used as the base liquid. Then, 16.00 g of NaCl, 4.28 g of $MgCl_2{\cdot}6H_2O$, 2.00 g of $CaCl_2$, and 2.40 g of Na_2CO_3 were sequentially added, followed by high-speed stirring for 10 min. Subsequently, 40.00 g of sodium bentonite was added, and the mixture was stirred at high speed for an additional 30 min. The prepared mud was aged at room temperature for 24 h to obtain the mixed-salt–based mud.

2.4.2 Preparation of Shale Gas Water-Based Drilling Fluids

According to the shale gas water-based drilling fluid formulation listed in Table 1, all components were sequentially added into a high-speed mixing cup under continuous stirring at 8000 r/min. The interval between successive additions was maintained at 5–10 min, and the feeding time for each component was controlled within 10–30 s. After the addition of the final component, the drilling fluid was further stirred for 30 min to obtain a homogeneous shale gas water-based drilling fluid.

Table 1: Formulation of shale gas water-based drilling fluid and functions of additives.

No.	Drilling Fluid Additive	Dosage	Function
1	Bentonite-based mud	70 mL freshwater-based mud + 280 mL deionized water (total volume: 350 mL)	Provides basic rheology and initial filter cake
2	Sodium hydroxide	1.05 g	pH adjustment
3	Lubricant	35.00 g	Reduces friction and improves lubricity
4	Encapsulating agent	0.70 g	Enhances shale cuttings integrity
5	Inorganic salt	21.00 g	Improves inhibition against shale hydration
6	Inhibitor	7.00 g	Strengthens dispersion inhibition
7	Organic salt	17.50 g	Antioxidation
8	Modified cellulose	As required	Rheology regulation and filtration control
9	Plugging agent	10.50 g	Enhances plugging performance
10	Barite	As required, to achieve the drilling fluid density of 1.80 g/cm^3	Density control

2.5 Performance Evaluation of Bentonite-Based Muds and Drilling Fluids

2.5.1 Rheological Property Evaluation

The rheological properties of the bentonite-based muds and drilling fluids were characterized in accordance with the American Petroleum Institute recommended practice (API RP 13I, 2004) using a six-speed rotational viscometer (ZNN-D6B, Qingdao Chuangmeng Instrument Technology Service Co., Ltd., China). Dial readings were recorded at rotational speeds of 600, 300, and 3 rpm and denoted as θ600, θ300, and θ3, respectively. Each sample was measured three times, and the average value was taken as the final result. Based on these measurements, the apparent viscosity (AV), plastic viscosity (PV), yield point (YP), and gel strength (GS@10s and GS@10m) were calculated according to the Bingham model using Eqs. (1)–(5). Furthermore, the ratio of YP to PV (YP/PV) was calculated to evaluate the velocity distribution characteristics of the fluid in the annular space of the wellbore. A higher YP/PV ratio generally corresponds to a flatter velocity profile, which is beneficial for enhancing cuttings suspension and transport efficiency [39].

$$AV = 0.5 \times \theta 600 \ (\mathrm{mPa \cdot s}) \tag{1}$$

$$PV = \theta 600 - \theta 300 \ (\mathrm{mPa \cdot s}) \tag{2}$$

$$YP = 0.511 \times (\theta 300 - PV) \ (\mathrm{Pa}) \tag{3}$$

$$\mathrm{GS@10s} = 0.511 \times \theta 3s (\mathrm{Pa}) \tag{4}$$

$$\mathrm{GS@10m} = 0.511 \times \theta 3m (\mathrm{Pa}) \tag{5}$$

GS@10s and GS@10m denote the gel strengths after static periods of 10 s and 10 min, respectively, expressed in Pa. θ3s and θ3m represent the corresponding maximum dial readings at 3 rpm. The value 0.511 is the instrument calibration constant in Pa per dial unit, used to convert dial readings into shear stress.

2.5.2 Filtration Control Performance Evaluation

The filtration control performance of drilling fluids was evaluated by measuring the volume of filtrate passing through a filter medium under specified pressure, temperature, and time conditions. Low-temperature low-pressure (LTLP) filtration tests were conducted in accordance with the American Petroleum Institute standard (API RP 13B-1, 2009). In this method, a differential pressure of 100 psi was applied at room temperature, and the filtrate volume was collected over a period of 30 min [40]. To further characterize the filtration behavior of drilling fluids under high-temperature and high-pressure conditions, high-temperature high-pressure (HTHP) filtration tests were performed using an HTHP filter press (GGS71, Qingdao Chuangmeng Instrument Technology Service Co., Ltd., China). The filtration volume was measured over 30 min under a differential pressure of 500 psi at the specified test temperature [41]. All experiments were performed in triplicate, and the data are presented as mean ± standard deviation.

2.6 Filter Cake Surface Morphology Characterization

The surface morphology of the filter cakes was examined using a field-emission scanning electron microscope (FE-SEM, SU8000, Hitachi, Japan). The observations were carried out at an accelerating voltage of 1.0 kV and a working distance of 8.0 mm. Images were acquired at magnifications of ×50 and ×250 using the low-magnification secondary electron imaging mode (LM(L)).

2.7 Zeta Potential Measurement

The zeta potential of the shale gas water-based drilling fluid systems was measured using a Zetasizer Nano Z (Malvern Instruments, UK) to evaluate the effect of PAC-g-(SVS/SMAS/MAA) on system stability. Prior to measurement, the drilling fluid samples were diluted tenfold with deionized water. All measurements were performed at room temperature. Each sample was tested in triplicate, and the results are presented as mean ± standard deviation.

3 Results and Discussion

3.1 Optimization of Synthesis Conditions

To elucidate the influence of synthesis parameters on the performance of PAC-g-(SVS/SMAS/MAA), mixed-salt–based mud was selected as the evaluation system. At a fixed additive dosage of 20 g/L, the rheological retention and filtration control performance of products synthesized under different conditions were systematically compared after aging at 160°C for 16 h, and the results are summarized in Fig. 3.

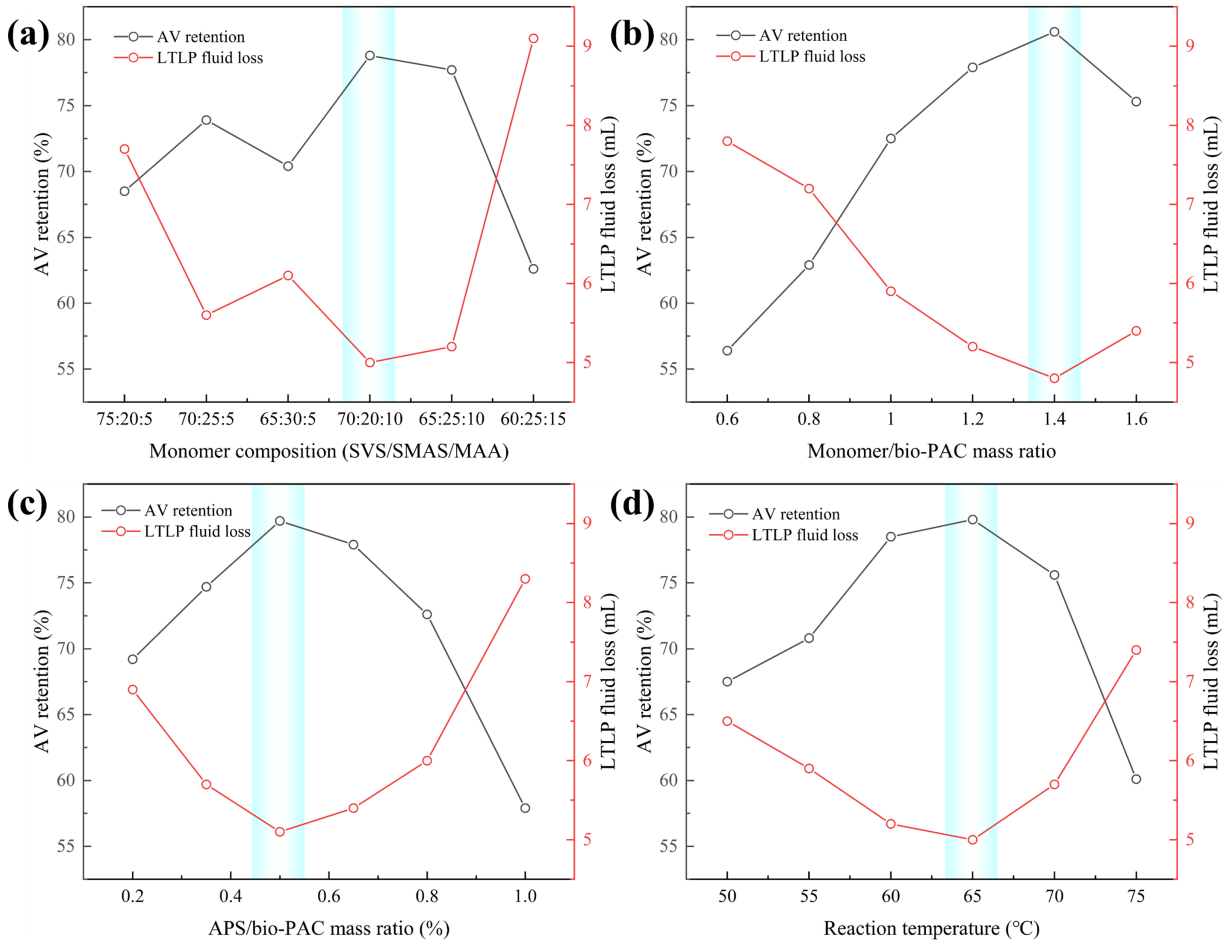

Figure 3: Effect of synthesis parameters on the performance of PAC-g-(SVS/SMAS/MAA): (**a**) monomer composition, (**b**) monomer/PAC mass ratio, (**c**) APS/bio-PAC mass ratio, and (**d**) reaction temperature.

Overall, monomer composition, grafting intensity, initiator dosage, and reaction temperature exerted significant effects on the comprehensive performance of the material in high-temperature mixed-salt environments; however, their underlying mechanisms differed markedly. First, the influence of monomer molar ratio was primarily associated with the balance of synergistic effects among hydrophilic ionic functional groups (Fig. 3a). As the MAA content increased from 5% to approximately 10%, both the AV retention and LTLP filtration control performance improved simultaneously, with the composition SVS/SMAS/MAA = 70:20:10 exhibiting the best overall performance. In contrast, a further increase in MAA content to 15% led to a pronounced deterioration in stability under mixed-salt conditions. This behavior suggests that an appropriate amount of carboxyl groups enhances polymer adsorption onto particle surfaces and facilitates network reconstruction, whereas excessive carboxylate content may induce unfavorable ionic bridging effects in Ca^{2+}- and Mg^{2+}-containing systems, thereby compromising structural stability after high-temperature aging.

Based on the optimized monomer composition, the regulatory role of grafting intensity on material performance became more evident (Fig. 3b). As the mass ratio of total monomers to bio-PAC increased from 0.6 to 1.4, the AV retention increased continuously, while the LTLP filtration volume decreased significantly,

indicating that a moderate increase in grafting density is beneficial for enhancing chain extension and film-forming capability. However, when the mass ratio was further increased to 1.6, a decline in performance was observed. This deterioration is likely attributable to structural heterogeneity or an increased proportion of free copolymers caused by excessive grafting, which is unfavorable for the formation of a stable and continuous polymer–particle network.

The initiator dosage also played a critical role in determining grafting efficiency (Fig. 3c). At low APS/bio-PAC ratios, insufficient initiation efficiency limited effective graft formation. Conversely, excessive APS promoted radical-induced degradation of the polysaccharide backbone and intensified side reactions, resulting in reduced high-temperature stability. In comparison, an APS/bio-PAC ratio of 0.50% provided an optimal balance between grafting efficiency and backbone integrity, enabling the material to achieve both high AV retention and low LTLP filtration loss.

The effect of reaction temperature reflects a combined balance among radical generation rate, monomer reactivity, and cellulose backbone stability (Fig. 3d). Within the temperature range of 50°C–65°C, material performance improved markedly with increasing temperature. When the temperature was further increased to 75°C, however, thermally induced backbone degradation became dominant, leading to a deterioration in overall performance. Therefore, a moderately elevated reaction temperature is more favorable for obtaining graft copolymers with uniform grafting and stable structures.

Based on the results shown in Fig. 3, the optimal synthesis window for PAC-g-(SVS/SMAS/MAA) was determined as follows: SVS/SMAS/MAA molar ratio of 70:20:10, monomer/bio-PAC mass ratio of 1.4, APS/bio-PAC mass ratio of 0.50%, and a reaction temperature of 65°C. Under these conditions, the material, when added at 20 g/L to mixed-salt–based mud and aged at 160°C for 16 h, maintained an AV retention of 81.3% and reduced the LTLP filtration volume to 4.6 mL. These results demonstrate that the optimized PAC-g-(SVS/SMAS/MAA) achieves a synergistic enhancement of rheological stability and filtration control performance under high-temperature and high-salinity conditions.

3.2 Characterization of PAC-g-(SVS/SMAS/MAA)

3.2.1 FT-IR Analysis

The FT-IR spectrum of PAC-g-(SVS/SMAS/MAA) prepared under the optimized conditions is shown in Fig. 4, revealing characteristic structural features of both the polysaccharide backbone and the grafted side chains. The broad absorption band centered at 3430 cm^{-1} is attributed to the stretching vibration of –OH groups originating from the cellulose backbone and its derivatives. This feature also indicates strong hydrophilicity and hydrogen-bonding capability, which are essential for effective hydration and rheological regulation in drilling fluid systems. The absorption peak at 2928 cm^{-1} can be assigned to the stretching vibrations of aliphatic C–H bonds ($–CH_2–$/$–CH_3$), suggesting that the introduction of grafted side chains does not disrupt the fundamental carbon–hydrogen framework of the polysaccharide backbone. The bands observed at 1606 and 1421 cm^{-1} correspond to the asymmetric and symmetric stretching vibrations of $–COO^-$ groups, respectively, confirming the successful incorporation of carboxylate functionalities. The absorption peak at 1326 cm^{-1} is associated with the deformation vibrations of $–CH_3$ and $–CH_2–$ groups, which originate from the alkyl structures introduced by MAA and sulfonate-containing monomers, further indicating the successful construction of grafted side chains. The characteristic peak at 1123 cm^{-1} is attributed to the stretching vibration of S=O bonds in sulfonate groups, while the band at 1013 cm^{-1} corresponds to the characteristic C–O–C stretching vibration of the cellulose ether backbone. The incorporation of sulfonate groups endows the material with enhanced salt resistance and hydration stability, providing a critical structural basis for maintaining rheological performance in high-salinity and mixed-salt drilling fluid

environments. In addition, the absorption band observed at 614 cm^{-1} can be assigned to the bending vibrations of C–S or S–O bonds, further confirming the presence of sulfur-containing functional groups. Overall, these results demonstrate that the PAC backbone retains the characteristic features of the polysaccharide structure while being successfully grafted with both carboxylate and sulfonate functional groups.

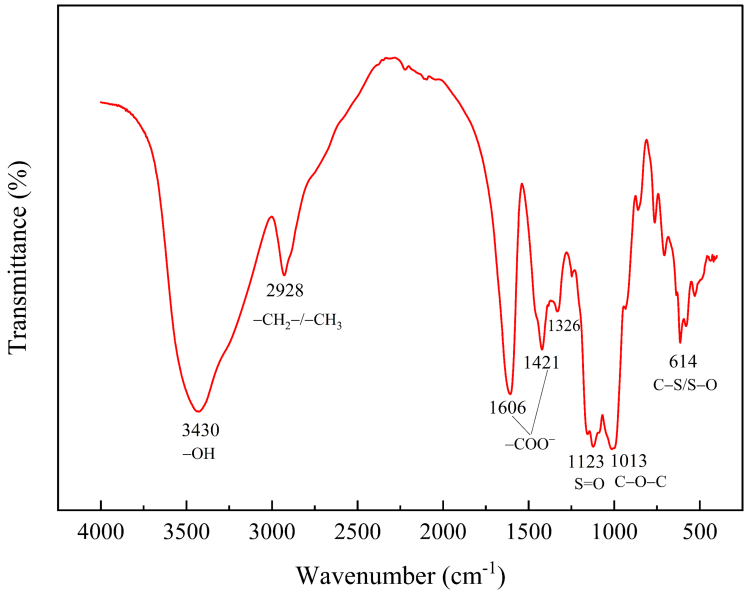

Figure 4: FT-IR spectrum of PAC-g-(SVS/SMAS/MAA).

3.2.2 Thermogravimetric Analysis

The TG–DTG curves of the synthesized PAC-g-(SVS/SMAS/MAA) are presented in Fig. 5, and the thermal decomposition process can be divided into three main stages. The first stage occurs in the temperature range of 30°C–330.7°C, with a mass loss of approximately 9.6%. This weight loss is mainly attributed to the evaporation of physically adsorbed moisture and a small amount of low-molecular-weight components, and no obvious degradation of the polymer backbone is observed during this stage. The second stage, located between 330.7°C and 370.1°C, corresponds to the primary mass-loss region in the TG curve. The onset and end temperatures of decomposition were determined using the tangent method applied to the TG curve [36]. A maximum decomposition rate peak appears at 357.9°C in the DTG curve, indicating rapid thermal decomposition of the polymer near this temperature. When the temperature reaches 370.1°C, the residual mass decreases to 57.7%, and the cumulative mass loss in this stage is approximately 32.7%. This mass loss is mainly associated with the cleavage of grafted side chains and the thermal decomposition of sulfonate groups [42]. The third stage occurs above 370°C, with a mass loss of approximately 5.9%, which can be attributed to further thermal degradation and carbonization of the polymer backbone. Overall, the TG–DTG results indicate that PAC-g-(SVS/SMAS/MAA) maintains high mass stability below 330°C under a nitrogen atmosphere, demonstrating good thermal stability. This behavior can be primarily ascribed to the three-dimensional network structure constructed on the cellulose backbone through graft modification, as well as the incorporation of sulfonate functional groups, which effectively enhance the thermal stability of the polymer chains. These features provide a solid thermal stability basis for the application of the material in high-temperature water-based drilling fluid systems.

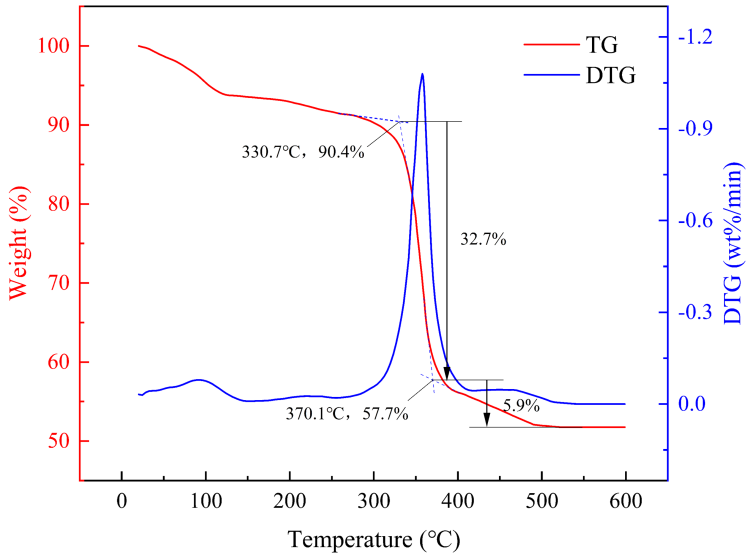

Figure 5: TG and DTG curves of PAC-g-(SVS/SMAS/MAA).

3.2.3 Biotoxicity Analysis

To evaluate the potential environmental impact of the synthesized PAC-g-(SVS/SMAS/MAA), biotoxicity tests were conducted to characterize its acute toxicity, with the half-maximal effective concentration (EC_{50}) used as the evaluation metric. EC_{50} represents the sample concentration that induces 50% of the maximum effect in the test organism within a specified exposure period. The results indicate that PAC-g-(SVS/SMAS/MAA) exhibits an EC_{50} value of 73,000 mg/L, which is significantly higher than both the non-toxic classification threshold ($EC_{50} \geq$ 25,000 mg/L) and the regulatory discharge requirement ($EC_{50} \geq$ 30,000 mg/L) [43]. This favorable biotoxicity performance is closely related to the structural characteristics and raw material origin of the material. On the one hand, the PAC backbone is derived from natural cellulose, whose biocompatibility and environmental friendliness have been extensively validated. On the other hand, the grafted sulfonate and carboxylate functional groups are water-soluble anionic moieties that are not prone to bioaccumulation or persistent toxic effects in aquatic environments, thereby satisfying environmental safety requirements for drilling fluid additives.

3.3 Performance Evaluation of PAC-g-(SVS/SMAS/MAA) in Bentonite-Based Muds

3.3.1 Thermal Resistance Evaluation

To systematically evaluate the rheological stability and filtration control capability of PAC-g-(SVS/SMAS/MAA) under high-temperature conditions, the polymer was added to mixed-salt–based mud at a dosage of 30 g/L. The samples were subjected to rolling aging at temperatures ranging from 25°C to 160°C for 16 h, after which their rheological parameters and LTLP filtration performance were measured. The results are presented in Fig. 6. All retention and increase ratios were calculated with reference to the data obtained at 25°C.

As shown in Fig. 6a–c, the AV, PV, and YP of the system gradually decreased with increasing aging temperature; however, the overall attenuation remained moderate. When the aging temperature was increased from 25°C to 120°C, the retention of the main rheological parameters remained at relatively high levels. Even after aging at 160°C, the retention rates of AV, PV, and YP were still 75.3%, 80.0%, and 66.7%, respectively. Meanwhile, the YP/PV ratio exhibited a slight decrease with increasing temperature, but its retention rate

remained as high as 83.3% at 160°C, indicating that high-temperature aging exerted a relatively limited influence on the flow behavior characteristics of the system. With respect to filtration performance (Fig. 6d), the LTLP filtration volume increased gradually with increasing aging temperature, rising from 2.4 mL at 25°C to 3.6 mL at 160°C, corresponding to an LTLP increase rate of 50.0%. Although high-temperature aging led to a certain increase in filtration volume, its absolute value remained at a low level throughout the tested temperature range. This observation suggests that the material can still effectively participate in filter cake formation and maintain satisfactory filtration control under high-temperature conditions.

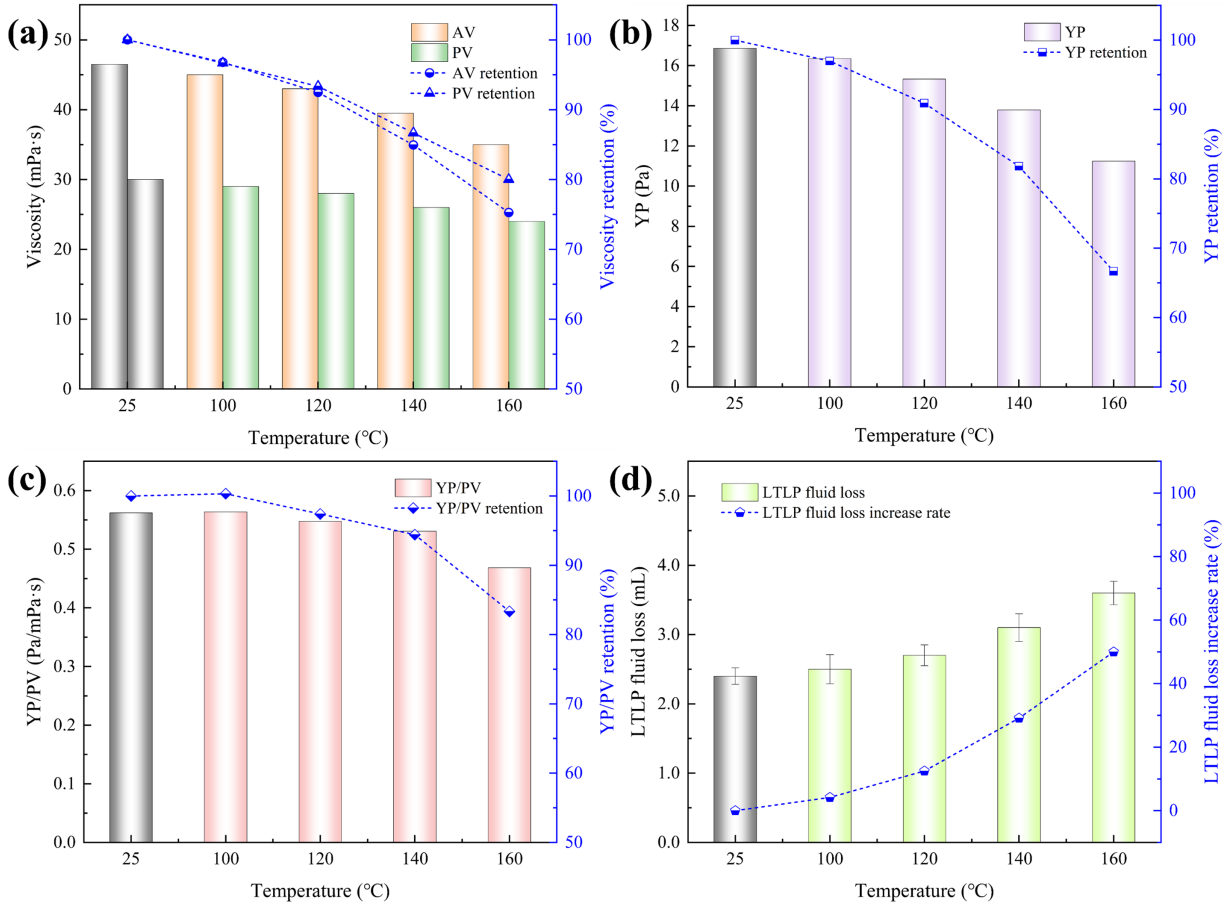

Figure 6: Thermal resistance of PAC-g-(SVS/SMAS/MAA) in composite brine-based mud: (**a**) AV and PV with corresponding retention, (**b**) YP with retention, (**c**) YP/PV with retention, and (**d**) LTLP fluid loss with increase rate.

Overall, these results demonstrate that PAC-g-(SVS/SMAS/MAA) exhibits good thermal resistance in mixed-salt–based muds. Even after high-temperature aging, the system retains relatively high rheological parameters and controllable filtration levels, reflecting the structural stability and promising application potential of this graft copolymer in high-temperature and high-salinity environments.

3.3.2 Performance Evaluation in Freshwater-Based Muds

Under fixed aging conditions of 160°C for 16 h, the effects of different dosages (0–30 g/L) of PAC-g-(SVS/SMAS/MAA) on the rheological behavior and filtration performance of freshwater-based muds were investigated. The results are shown in Fig. 7. All increase and reduction ratios were calculated with reference to the untreated system (0 g/L).

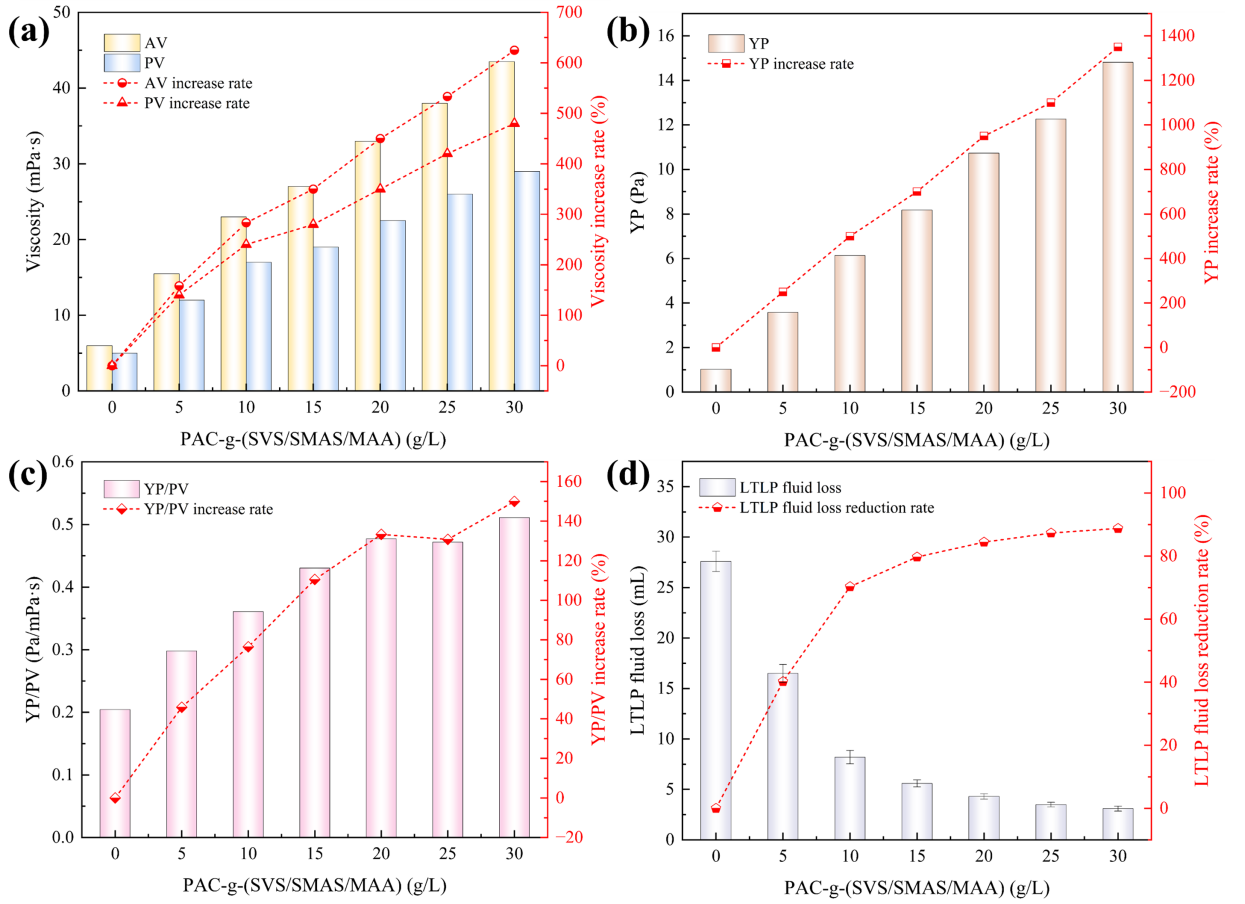

Figure 7: Effect of PAC-g-(SVS/SMAS/MAA) dosage on the performance of freshwater-based mud after aging at 160°C for 16 h: (**a**) AV and PV with increase rate, (**b**) YP with increase rate, (**c**) YP/PV with increase rate, and (**d**) LTLP fluid loss with reduction rate.

As illustrated in Fig. 7a–c, the rheological parameters of the freshwater-based muds after aging at 160°C for 16 h exhibited a pronounced enhancement with increasing PAC-g-(SVS/SMAS/MAA) dosage from 0 to 30 g/L. The AV, PV, and YP increased markedly with dosage, with particularly significant improvements observed in the low-dosage range (≤20 g/L). At a dosage of 20 g/L, AV, PV, and YP increased to 33.0 mPa·s, 22.5 mPa·s, and 10.7 Pa, corresponding to increase rates of 450.0%, 350.0%, and 950.0%, respectively. Meanwhile, the YP/PV ratio showed an overall upward trend with increasing dosage and remained at relatively high levels in the medium-to-high dosage range. This behavior indicates that, while substantially enhancing system viscosity, the polymer also effectively strengthens the structural integrity and improves the flow characteristics of the drilling fluid. As the dosage was further increased to 25–30 g/L, the rheological parameters continued to increase; however, the rate of improvement gradually diminished, suggesting that the system was approaching an effective upper limit for rheological enhancement.

In terms of filtration performance (Fig. 7d), the LTLP filtration volume decreased significantly with increasing PAC-g-(SVS/SMAS/MAA) dosage. At 20 g/L, the LTLP filtration volume was reduced from 27.6 mL for the untreated system to 4.3 mL, corresponding to an LTLP reduction rate of 84.4%. When the dosage was further increased to 30 g/L, the LTLP value decreased only slightly to 3.1 mL, indicating that the filtration control performance tended to level off at higher dosages.

Overall, PAC-g-(SVS/SMAS/MAA) exhibits a pronounced synergistic effect on viscosity enhancement and filtration reduction in freshwater-based muds. With increasing dosage, both rheological parameters and filtration performance are significantly improved; however, the performance enhancement gradually plateaus beyond 20 g/L, suggesting the existence of a reasonable and effective dosage window for this material in freshwater-based mud systems.

3.3.3 Performance Evaluation in Saturated Brine–Based Muds

To assess the salt tolerance of the synthesized material, the effects of different dosages of PAC-g-(SVS/SMAS/MAA) on the rheological behavior and LTLP filtration performance of saturated brine–based muds were further investigated under identical high-temperature aging conditions. The results are presented in Fig. 8.

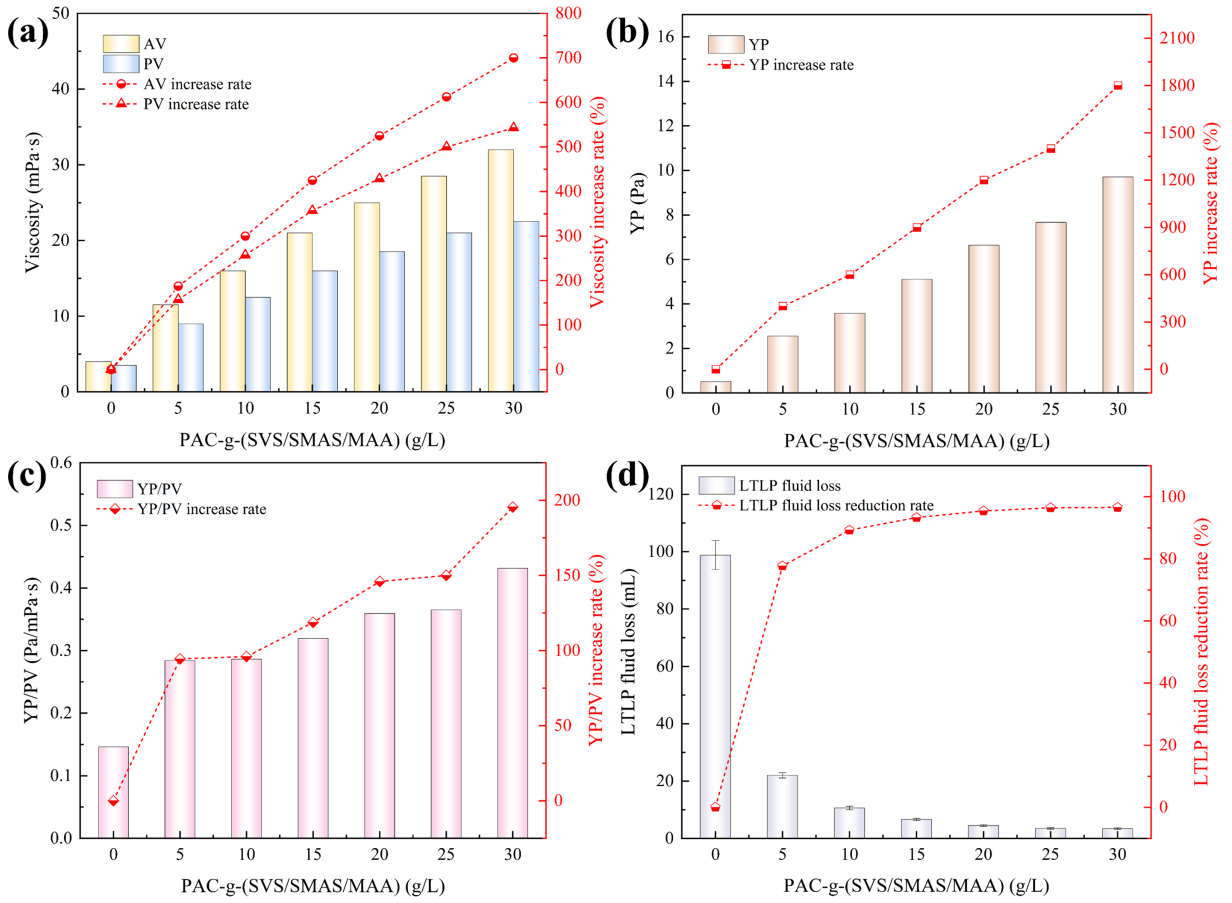

Figure 8: Effect of PAC-g-(SVS/SMAS/MAA) dosage on the performance of saturated brine-based mud after aging at 160°C for 16 h: (**a**) AV and PV with increase rate, (**b**) YP with increase rate, (**c**) YP/PV with increase rate, and (**d**) LTLP fluid loss with reduction rate.

As shown in Fig. 8a,b, the rheological parameters of the saturated brine–based muds exhibited a continuous increase with increasing PAC-g-(SVS/SMAS/MAA) dosage; however, their absolute values remained lower than those observed in the freshwater-based mud system, reflecting the inhibitory effect of high salinity on polymer hydration and structural development. Nevertheless, the material still demonstrated a pronounced viscosity-enhancing effect. At a dosage of 20 g/L, AV, PV, and YP increased to 25.0 mPa·s,

18.5 mPa·s, and 6.6 Pa, corresponding to increase rates of 525.0%, 428.6%, and 1200.0%, respectively. With further increases in dosage, all rheological parameters continued to rise, although the rate of improvement gradually diminished.

Meanwhile, the YP/PV ratio of the system exhibited an overall increasing trend with increasing dosage (Fig. 8c) and remained at relatively high levels in the medium-to-high dosage range. This behavior indicates that, even in saturated brine environments, PAC-g-(SVS/SMAS/MAA) not only enhances viscosity but also effectively strengthens the structural integrity and improves the flow behavior of the system.

In terms of filtration performance (Fig. 8d), the LTLP filtration volume decreased significantly with increasing additive dosage, dropping rapidly from 98.8 mL in the untreated system to 4.5 mL at a dosage of 20 g/L, corresponding to an LTLP reduction rate of 95.4%. When the dosage was further increased to 25–30 g/L, the filtration volume decreased only slightly and tended to stabilize, indicating that a dense and stable filter cake structure had already been established at higher dosages.

Overall, the results in Fig. 8 demonstrate that, although the saturated brine environment markedly weakens the baseline rheological properties of the system, PAC-g-(SVS/SMAS/MAA) still exhibits excellent viscosity enhancement and filtration reduction capabilities. Notably, at dosages of 20 g/L and above, the material can substantially improve the rheological structure and filtration control performance of saturated brine–based muds, highlighting its good adaptability to high-salinity conditions.

3.3.4 Performance Evaluation in Mixed-Salt–Based Muds

Mixed-salt–based muds contain not only high concentrations of Na^+ but also divalent cations such as Ca^{2+} and Mg^{2+}, which impose more stringent requirements on polymer hydration, conformational stability, and adsorption-induced film formation. Under fixed aging conditions (160°C for 16 h), the regulatory effects of different dosages of PAC-g-(SVS/SMAS/MAA) on the rheological behavior and LTLP filtration performance of mixed-salt–based muds were investigated, and the results are shown in Fig. 9.

As illustrated in Fig. 9a,b, compared with freshwater and single-salt systems, the mixed-salt environment exerts a more pronounced inhibitory effect on polymer hydration and structural development. Nevertheless, the material still exhibits a strong viscosity-enhancing capability. At a dosage of 20 g/L, AV, PV, and YP increased to 26.0 mPa·s, 18.5 mPa·s, and 7.7 Pa, respectively. Although these absolute values are lower than those obtained in freshwater systems, they represent a substantial improvement relative to the untreated base mud, indicating that the material retains effective hydration and structural support capabilities even under strong electrolyte conditions. In addition, the YP/PV ratio of the system increases overall with increasing dosage (Fig. 9c) and remains within a reasonable range at medium-to-high dosages, suggesting that the enhancement in viscosity does not lead to severe deterioration of flow behavior and remains favorable for stable fluid transport in the wellbore annulus.

With respect to filtration control (Fig. 9d), the LTLP filtration volume of the mixed-salt–based mud reaches as high as 126.6 mL in the absence of additives, indicating that the system is almost incapable of forming an effective filter cake under conditions where multivalent ions coexist. Upon the introduction of PAC-g-(SVS/SMAS/MAA), the filtration volume decreases markedly with increasing dosage. At 20 g/L, the LTLP filtration volume is reduced to 4.8 mL, corresponding to an LTLP reduction rate of 96.2%. When the dosage is further increased to 25–30 g/L, the filtration volume changes only slightly and tends to stabilize, indicating that a dense and stable filtration-control structure has already been established.

Overall, even in complex systems containing multiple inorganic salts, PAC-g-(SVS/SMAS/MAA) is capable of simultaneously enhancing rheological parameters and effectively suppressing filtration loss. These

results demonstrate the excellent salt-tolerance adaptability and promising application potential of this material under complex high-salinity conditions.

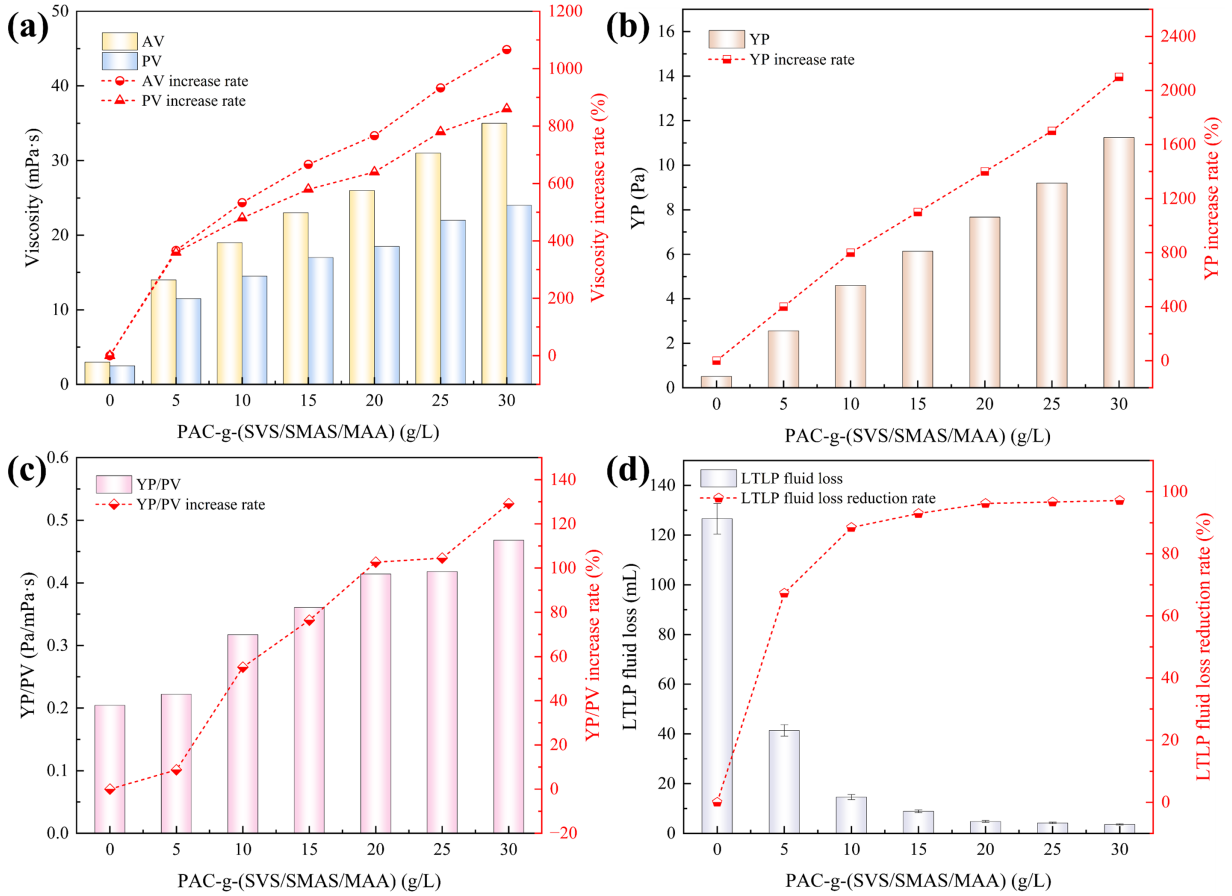

Figure 9: Effect of PAC-g-(SVS/SMAS/MAA) dosage on the performance of composite brine-based mud after aging at 160°C for 16 h: (**a**) AV and PV with increase rate, (**b**) YP with increase rate, (**c**) YP/PV with increase rate, and (**d**) LTLP fluid loss with reduction rate.

3.4 Performance Evaluation of PAC-g-(SVS/SMAS/MAA) in Shale Gas Water-Based Drilling Fluids

In the aforementioned bentonite-based mud systems, PAC-g-(SVS/SMAS/MAA) has demonstrated excellent thermal resistance, salt tolerance, and rheology–filtration regulation capability. However, practical shale gas water-based drilling fluids are typically composed of multiple functional additives, resulting in a more complex system in which performance is governed by the synergistic and competitive interactions among different components. To further assess the application potential of this material under engineering-relevant conditions, its dosage-dependent performance and comparative behavior relative to commercial modified cellulose products were investigated using a shale gas water-based drilling fluid formulation.

3.4.1 Effect of Dosage on Rheological and Filtration Performance

Under the specified shale gas water-based drilling fluid formulation, the effects of PAC-g-(SVS/SMAS/MAA) dosage on rheological behavior and filtration control performance were systematically evaluated after aging at 160°C for 16 h, with the aim of identifying a reasonable and effective dosage range for practical applications. The results are shown in Fig. 10.

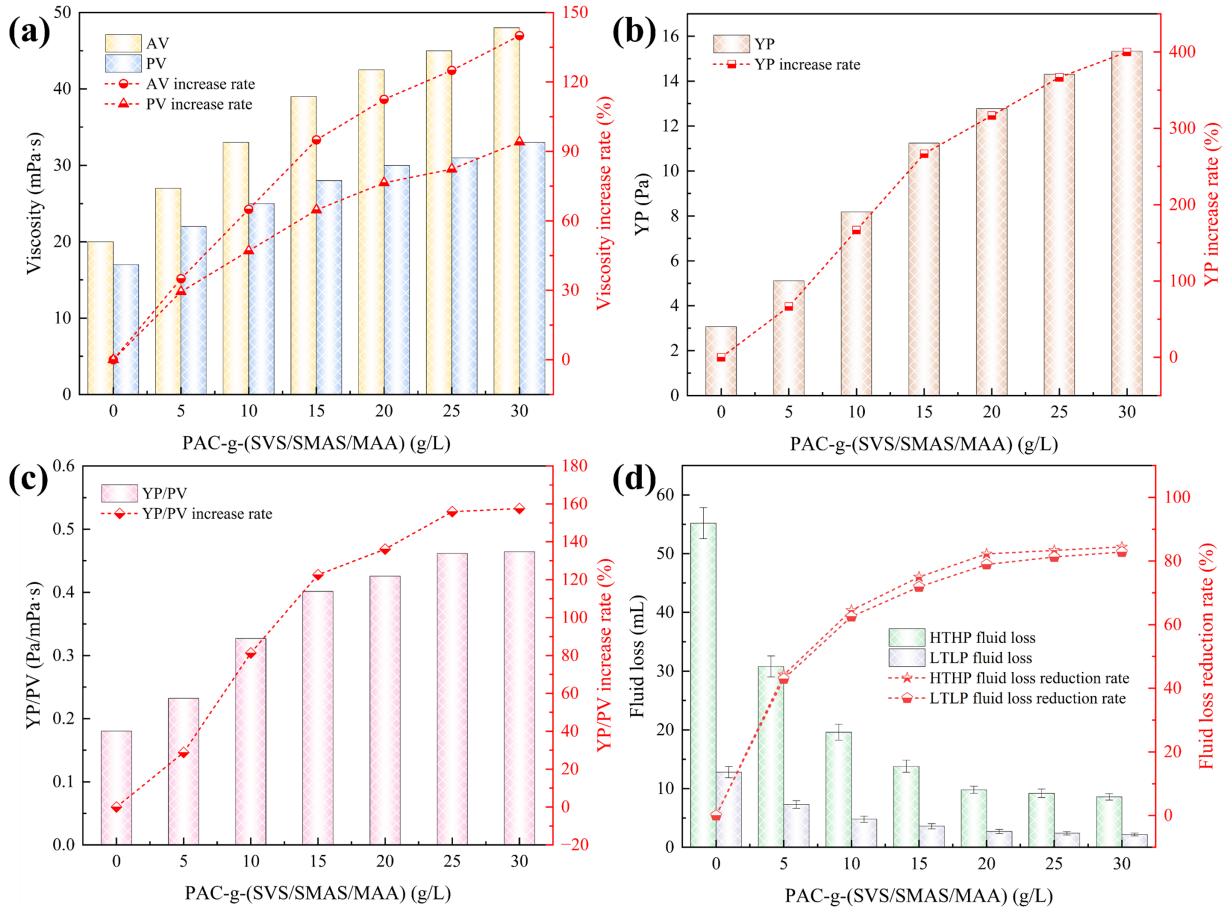

Figure 10: Effect of PAC-g-(SVS/SMAS/MAA) dosage on the performance of shale gas water-based drilling fluid after aging at 160°C for 16 h: (**a**) AV and PV with increase rate, (**b**) YP with increase rate, (**c**) YP/PV with increase rate, and (**d**) LTLP and HTHP fluid loss with reduction rate.

As illustrated in Fig. 10a–c, in the absence of PAC-g-(SVS/SMAS/MAA), the drilling fluid exhibits a certain level of baseline rheological properties, but its structural strength remains limited. With the introduction of the polymer, the AV, PV, and YP are all significantly improved, indicating that PAC-g-(SVS/SMAS/MAA) can further reinforce the existing rheological framework of the system. When the dosage is increased from 0 to 20 g/L, the enhancement of all rheological parameters is most pronounced. At higher dosages, although the parameters continue to increase, the rate of improvement decreases markedly, suggesting that the system is gradually approaching an effective upper limit for structural development.

Meanwhile, the YP/PV ratio exhibits an overall upward shift with increasing dosage (Fig. 10c), indicating that, while enhancing the viscosity level, PAC-g-(SVS/SMAS/MAA) also contributes to improved flow behavior and enhanced shear-thinning characteristics. Such changes are beneficial for cuttings transport and annular stability in shale gas drilling operations. The filtration control results further support these observations (Fig. 10d). In the absence of the additive, both LTLP and HTHP filtration volumes of the drilling fluid remain at relatively high levels. Upon the addition of PAC-g-(SVS/SMAS/MAA), the filtration volumes decrease significantly and exhibit a clear inflection point at approximately 20 g/L. Further increases in dosage result in only marginal improvements in filtration performance, indicating that a stable and compact filter cake structure has already been established.

Based on these results, PAC-g-(SVS/SMAS/MAA) achieves an optimal balance between rheological regulation and filtration control at a dosage of approximately 20 g/L in shale gas water-based drilling fluid systems. Considering both engineering applicability and material utilization efficiency, this dosage was selected for subsequent comparative evaluations against commercial modified cellulose products.

3.4.2 Performance Comparison with Commercial Modified Cellulose Products

Based on the above results, a systematic comparison was conducted at the optimized dosage (20 g/L) to evaluate the effects of different cellulose-based additives on the rheological behavior and filtration performance of shale gas water-based drilling fluids under high-temperature aging conditions. The comparative results as a function of aging temperature are summarized in Fig. 11.

As shown in Fig. 11, distinct differences are observed among the cellulose-based additives in their ability to maintain drilling fluid performance under high-temperature aging conditions. With increasing aging temperature, the rheological structure of the drilling fluid without modified cellulose deteriorates rapidly. After aging at 180°C, its AV, PV, and YP decrease to 10.5 mPa·s, 10.0 mPa·s, and 0.5 Pa, respectively, corresponding to retention rates of only 35.0%, 40.0%, and 10.0%. Under these conditions, the system nearly loses its effective load-bearing capacity. Upon the addition of commercial HEC, the drilling fluid can maintain a certain level of rheological performance at 160°C; however, at 180°C, its AV and YP decrease to 14.0 mPa·s and 2.0 Pa, respectively, with retention rates of only 33.3% and 22.2%, indicating limited thermal adaptability. In comparison, commercial PAC exhibits relatively better stability at elevated temperatures; nevertheless, after aging at 180°C, its AV and YP still decrease to 16.5 mPa·s and 2.6 Pa, respectively, with retention rates below 40%.

In contrast, the drilling fluid treated with PAC-g-(SVS/SMAS/MAA) exhibits the highest rheological retention throughout the entire tested temperature range. Even after aging at 180°C, its AV, PV, and YP remain at 33.5 mPa·s, 25.0 mPa·s, and 8.7 Pa, respectively, corresponding to retention rates of 69.1%, 71.4%, and 63.0% (Fig. 11a–c), which are markedly higher than those of the commercial HEC- and PAC-treated systems. Further comparison of the YP/PV ratio (Fig. 11d) reveals that the flow behavior of the untreated and commercial HEC-treated systems deteriorates substantially after high-temperature aging. By contrast, the PAC-g-(SVS/SMAS/MAA)–treated system maintains a YP/PV ratio in the range of 0.35–0.43 at 160°C–180°C, with retention rates close to or exceeding 90%. This behavior is favorable for maintaining flow stability and efficient cuttings transport under high-temperature conditions.

As shown by the gel strength results (Fig. 11e,f), the structural recovery capability of different systems exhibits pronounced differences after aging at elevated temperatures. The GS@10s and GS@10m values of the blank system decrease rapidly with increasing aging temperature and both drop to 0 Pa after aging at 180°C, indicating a complete loss of static structural support under severe thermal aging conditions. The system containing commercial HEC shows measurable gel strength at lower aging temperatures; however, its GS values also decrease to 0 Pa after aging at 180°C, suggesting limited ability to maintain structural recovery after high-temperature aging. In comparison, the system with commercial PAC retains finite gel strength after aging (GS@10s and GS@10m of 0.26 and 0.51 Pa, respectively); however, the overall values remain low, indicating that its structural stability is still considerably weakened under high-temperature aging conditions. In contrast, the system containing PAC-g-(SVS/SMAS/MAA) maintains relatively high gel strength over the entire aging temperature range. Even after aging at 180°C, the GS@10s and GS@10m values reach 2.56 and 4.09 Pa, respectively, which are notably higher than those of the other systems. This indicates that the modified polymer is capable of sustaining a robust three-dimensional network structure and structural recovery ability after thermal aging, which is beneficial for suspending solid particles and preventing sedimentation under static conditions. Meanwhile, the GS@10m values are consistently higher

than the GS@10s values, reflecting effective structure-building capability. In addition, a moderate increase in gel strength (i.e., the difference between initial and final gel strength) helps avoid excessive structural rigidity that may lead to high startup resistance, thereby achieving a balance between suspension stability and flow recovery.

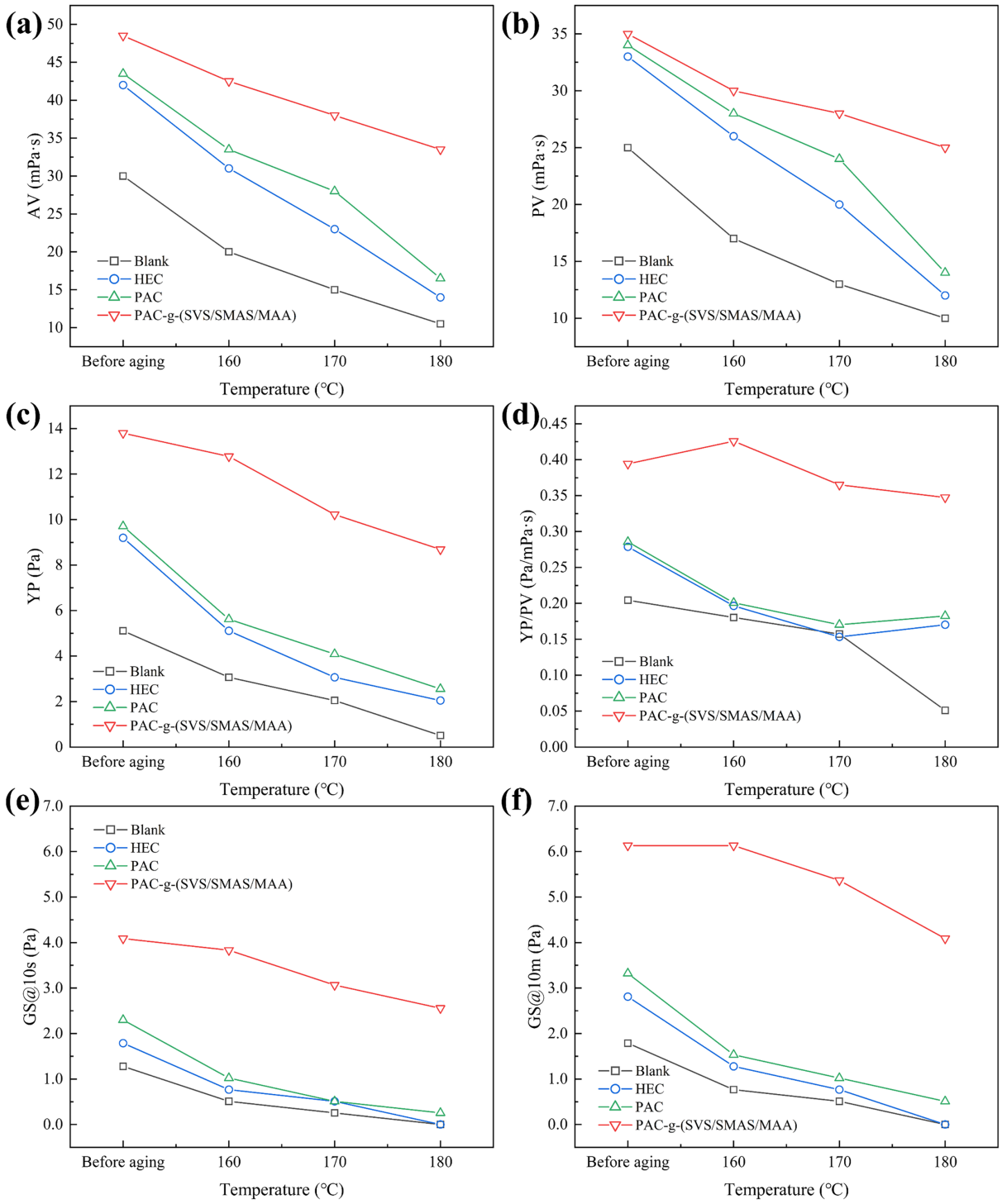

Figure 11: (Continued)

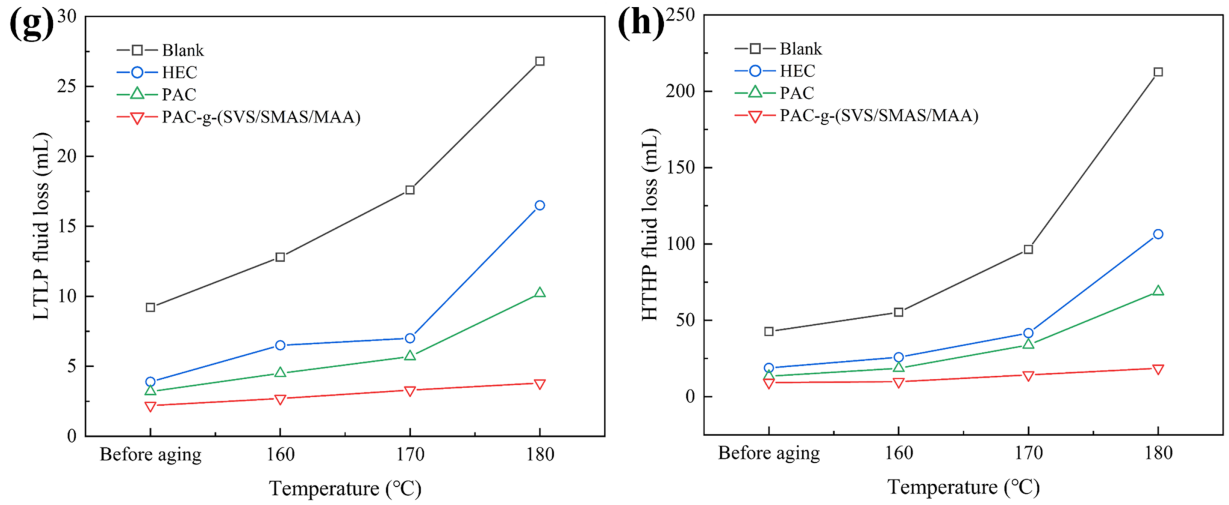

Figure 11: Performance comparison of PAC-g-(SVS/SMAS/MAA) with commercial modified celluloses in shale gas water-based drilling fluid: (**a**) AV, (**b**) PV, (**c**) YP, (**d**) YP/PV, (**e**) GS@10s, (**f**) GS@10m, (**g**) LTLP fluid loss, and (**h**) HTHP fluid loss. The dosage of each modified cellulose was 20 g/L.

With respect to filtration control (Fig. 11g,h), the drilling fluid without modified cellulose exhibits a sharp increase in filtration after aging at 180°C, with LTLP and HTHP filtration volumes rising to 26.8 and 212.6 mL, respectively, indicating an almost complete loss of effective filtration control. Although the commercial HEC- and PAC-treated systems can suppress filtration to some extent, their LTLP values remain above 10 mL and their HTHP filtration volumes exceed 60 mL. In contrast, under the same conditions, the PAC-g-(SVS/SMAS/MAA)–treated drilling fluid exhibits LTLP and HTHP filtration volumes of only 3.8 and 18.6 mL, respectively, demonstrating a pronounced advantage.

Overall, at the same dosage, PAC-g-(SVS/SMAS/MAA) simultaneously achieves high levels of rheological retention and excellent filtration control in high-temperature shale gas water-based drilling fluids. Its thermal stability is clearly superior to that of commercial HEC and PAC, highlighting its strong potential for practical engineering applications.

3.5 Mechanism of PAC-g-(SVS/SMAS/MAA)

3.5.1 Microstructural Analysis of Filter Cakes

Fluid loss in drilling fluids is essentially governed by the structural integrity of the filter cake and the connectivity of its pore network. After aging at 180°C, the HTHP filter cake formed by the drilling fluid without modified cellulose exhibits a rough surface with numerous irregular pores and localized collapse features (Fig. 12a1,a2). This observation indicates that, under high-temperature conditions, the system fails to establish a continuous and effective solid–polymer framework, resulting in interconnected pores and abundant seepage pathways. Consequently, an extremely high HTHP filtration volume of 212.6 mL is observed.

Upon the addition of commercial PAC, the overall continuity of the filter cake is improved, and both the size and number of pores are markedly reduced (Fig. 12b1,b2). Correspondingly, the HTHP filtration volume decreases to 68.8 mL, suggesting that PAC can promote solid particle packing and pore filling through adsorption and bridging interactions. Nevertheless, dispersed micropores and localized cracks are still evident at 180°C, indicating that the compactness and thermal stability of the filter cake formed by commercial PAC remain limited under such severe conditions.

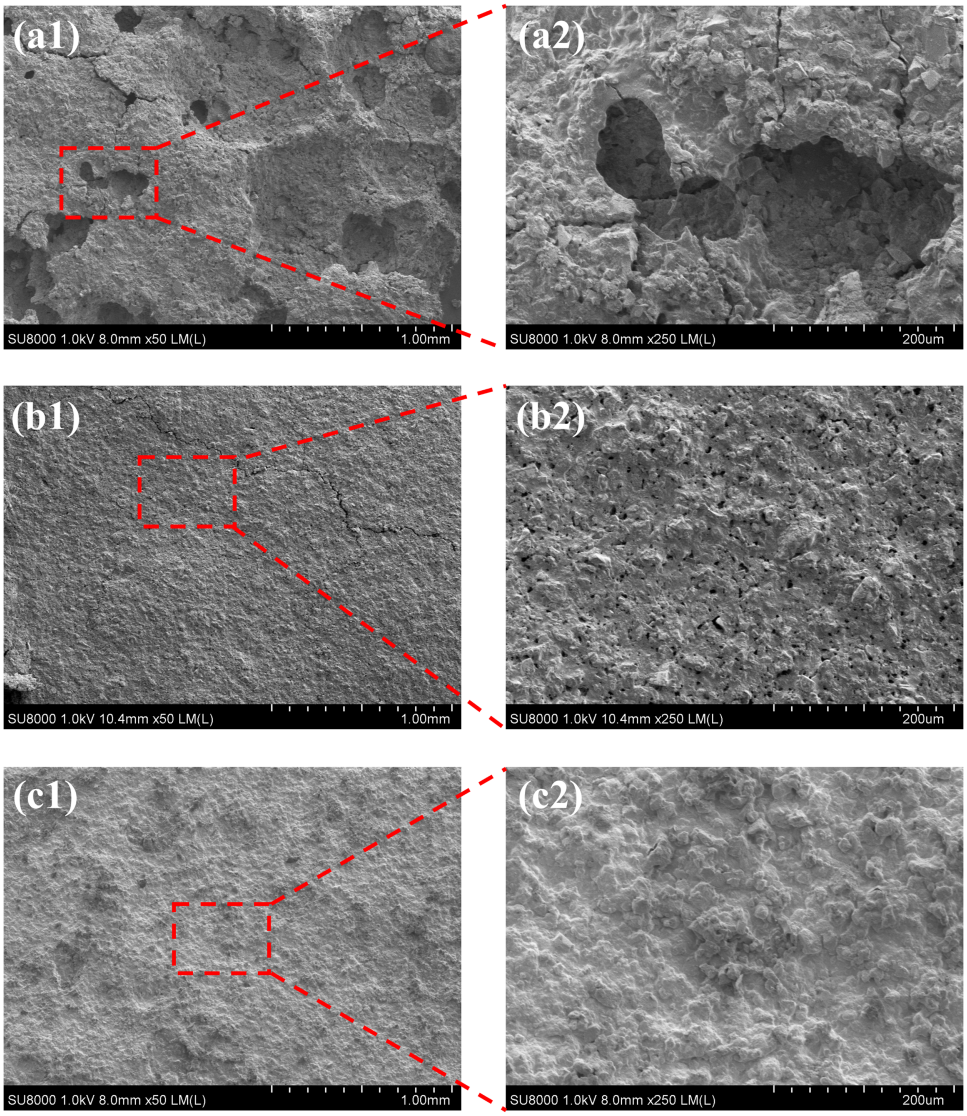

Figure 12: SEM images of HTHP mud cakes formed from shale gas water-based drilling fluids under different treatments after aging at 180°C: (**a**) without modified cellulose, (**b**) with 20 g/L PAC, and (**c**) with 20 g/L PAC-g-(SVS/SMAS/MAA). (**a1–c1**) and (**a2–c2**) correspond to magnifications of 50× and 250×, respectively.

In contrast, the filter cake formed in the presence of PAC-g-(SVS/SMAS/MAA) exhibits a much smoother and more continuous surface morphology at low magnification (Fig. 12c1). At higher magnification, the pores are significantly reduced in number and tend to become isolated (Fig. 12c2). These features demonstrate that PAC-g-(SVS/SMAS/MAA) effectively promotes dense packing of solid particles and the formation of a more stable polymer–particle composite structure under high-temperature and high-pressure conditions, thereby efficiently disrupting seepage pathways for filtrate flow under differential pressure. Consistent with these observations, the corresponding HTHP filtration volume is further reduced to 18.6 mL, which is markedly lower than that of the commercial PAC-treated system.

Overall, these results indicate that the advantage of PAC-g-(SVS/SMAS/MAA) lies not only in its viscosity-enhancing effect, but more importantly in its ability to construct dense, low-permeability filter cakes under high-temperature conditions.

3.5.2 Zeta Potential Analysis

The zeta potential results of the shale gas water-based drilling fluid systems at different aging temperatures are presented in Fig. 13. It can be observed that, with increasing aging temperature, the absolute values of zeta potential for all systems gradually decrease, indicating a progressive weakening of electrostatic stabilization under high-temperature conditions.

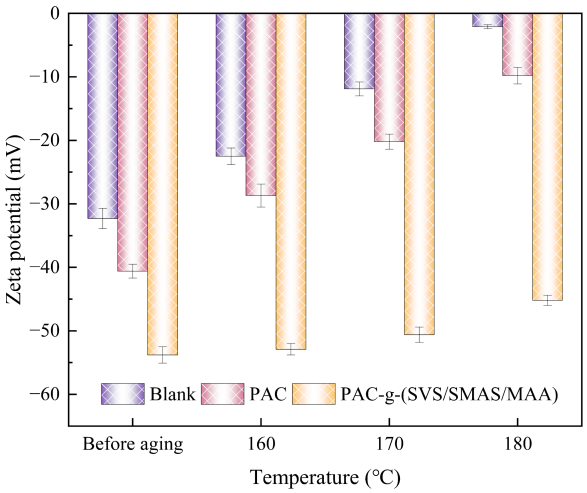

Figure 13: Zeta potential of shale gas water-based drilling fluid systems with different additives before and after aging at various temperatures.

For the blank system, the zeta potential decreases sharply from −32.3 mV before aging to −2.1 mV after aging at 180°C, indicating a significant reduction in electrostatic repulsion between particles. As a result, the system tends toward instability, leading to particle aggregation and structural collapse. This trend is consistent with the pronounced deterioration in rheological properties and the substantial increase in fluid loss observed under high-temperature conditions. After the addition of commercial PAC, the zeta potential values of the system remain lower (i.e., larger in absolute value) than those of the blank system over the entire temperature range, suggesting an improvement in particle dispersion. However, the absolute values still decrease noticeably with increasing aging temperature (from −40.6 to −9.8 mV), indicating that the electrostatic stabilization provided by PAC is still weakened to some extent under high-temperature and high-salinity conditions. In contrast, the system containing PAC-g-(SVS/SMAS/MAA) maintains relatively high absolute zeta potential values even after high-temperature aging, with the zeta potential decreasing only slightly from −53.8 to −45.2 mV. This small variation indicates that strong electrostatic repulsion is effectively preserved within the system. This behavior can be attributed to the grafted sulfonate groups, which exhibit strong ionization capability and stable charge characteristics, making them less susceptible to complete screening in high-salinity environments. As a result, a stable hydration layer around the polymer chains and a well-dispersed particle state can be maintained.

The enhanced electrostatic stabilization not only suppresses particle aggregation but also influences particle packing behavior during filter cake formation, promoting more uniform arrangement and denser packing of particles, thereby reducing pore connectivity. This observation is consistent with the SEM results, which show a more continuous and compact filter cake structure, as well as significantly reduced fluid loss. These findings further support, from the perspective of interfacial electrostatic properties, the proposed mechanisms involving polymer bridging, pore filling, and the formation of a dense filter cake.

3.5.3 Mechanism Analysis

Based on the combined results of rheological behavior, filtration performance, and filter cake SEM characterization, the performance advantages of PAC-g-(SVS/SMAS/MAA) in high-temperature shale gas water-based drilling fluids do not originate from a single mechanism. Instead, they arise from the synergistic contribution of solution-scale structural stabilization and interfacial-scale particle regulation. A schematic illustration of the proposed mechanism is shown in Fig. 14.

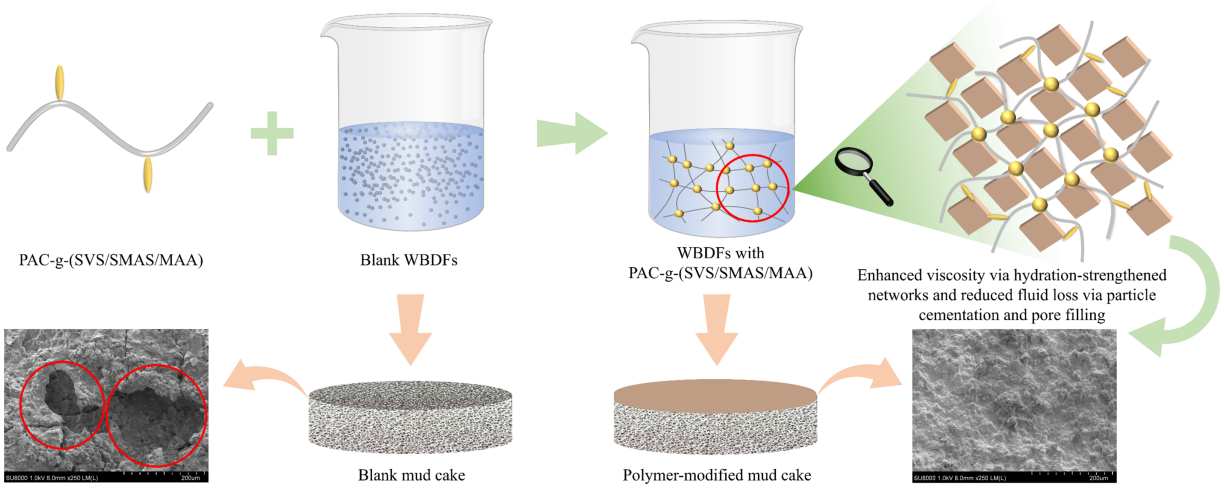

Figure 14: Schematic illustration of the working mechanisms of PAC-g-(SVS/SMAS/MAA) in shale gas water-based drilling fluids.

(1) Solution-scale structural stabilization: enhanced hydration and resistance to salt screening by strongly hydrophilic ionic groups

Commercial PAC mainly relies on carboxymethyl groups along the cellulose backbone to provide hydrophilicity and limited electrostatic repulsion. Under high-salinity conditions, however, effective charge screening by electrolytes markedly compresses the polymer coils, reduces the thickness of the hydration layer, and accelerates conformational collapse of polymer chains at elevated temperatures. As a result, the viscosity and structural strength of the system deteriorate rapidly. In contrast, PAC-g-(SVS/SMAS/MAA) introduces a high density of sulfonate groups (SVS/SMAS) together with carboxylate groups (MAA) onto the cellulose backbone via graft copolymerization. Among these functionalities, sulfonate groups exhibit stronger ionization capability and a more stable charge state, making them less susceptible to complete electrostatic screening in high-salinity environments. Consequently, a thicker and more stable hydration layer can be maintained around the polymer chains. Moreover, the distributed multivalent ionic groups along the polymer backbone significantly enhance interchain electrostatic repulsion and solvation effects, allowing the polymer chains to retain a relatively extended conformation even under high-temperature and high-salinity conditions. This structural feature effectively mitigates the combined compressive effects of salt ions and temperature on polymer coils, enabling PAC-g-(SVS/SMAS/MAA) to maintain high yield point and gel strength values after aging at 160°C–180°C. Such solution-scale stabilization provides a robust rheological foundation for stable solid suspension and overall structural integrity of the drilling fluid.

(2) Interfacial adsorption and bridging: multifunctional groups promoting particle cohesion and pore filling,

In complex shale gas water-based drilling fluid systems containing multiple solid phases and functional additives, drilling fluid performance depends not only on bulk rheological behavior but also critically on polymer adsorption at solid surfaces and its ability to regulate particle packing structures. For commercial PAC, adsorption mainly arises from limited interactions associated with hydroxyl and carboxymethyl groups. Under high-temperature conditions, the stability of the adsorption layer and the bridging capability tend to deteriorate due to polymer desorption or conformational collapse, resulting in loose filter cake structures and increased pore connectivity. By contrast, PAC-g-(SVS/SMAS/MAA) simultaneously possesses hydroxyl groups on the cellulose backbone as well as carboxylate and sulfonate groups on the grafted side chains, enabling multipoint and multiform cooperative adsorption onto bentonite platelets, weighting materials, and other solid surfaces. At the particle scale, this multifunctional architecture facilitates effective "bridging–cementation" interactions between adjacent particles, thereby enhancing interparticle connectivity and the stability of the spatial network. During filter cake formation, polymer chain bridging further restricts fine particle migration and promotes progressive pore filling and closure. In particular, under high-temperature conditions, the thermal stability and strong hydration capability of sulfonate groups help preserve the integrity of the adsorption layer and suppress localized "erosion–rearrangement" phenomena during filter cake buildup, resulting in a more continuous and homogeneous filter cake structure.

3.6 Limitations and Future Perspectives

Although the present study demonstrates that PAC-g-(SVS/SMAS/MAA) exhibits promising rheological regulation, filtration control, and thermal–salt resistance in shale gas water-based drilling fluids, several limitations should be recognized. First, the evaluation was conducted under controlled laboratory conditions, which may not fully capture the complexity of field operations, including dynamic flow, pressure variations, and formation heterogeneity. Second, while the macroscopic performance and interfacial electrostatic behavior were systematically analyzed, the underlying interactions among polymer chains, dissolved ions, and solid particles at the molecular level remain insufficiently clarified. In addition, the molecular weight characteristics of the grafted polymer were not determined, which may limit a deeper understanding of its structure–performance relationship. Furthermore, the long-term stability of the material under prolonged high-temperature conditions has not been fully assessed.

Future work should focus on addressing these limitations. Field-scale validation and compatibility evaluation with more complex drilling fluid formulations are necessary to confirm practical applicability. Advanced characterization techniques, together with molecular simulation approaches, are expected to provide further insight into the interaction mechanisms governing system stability and performance. In addition, molecular weight characterization should be incorporated to better establish correlations between polymer structure and functional properties. Optimization of monomer composition and grafting architecture may also enable improved performance under more extreme conditions. Finally, systematic evaluation of environmental impact, biodegradability, and economic feasibility will be important for facilitating the practical application of such biomass-derived polymer additives.

4 Conclusions

In this study, a high-temperature- and salt-resistant modified polymer, PAC-g-(SVS/SMAS/MAA), was synthesized using biomass-derived polyanionic cellulose (bio-PAC) as the backbone via free-radical graft copolymerization, in which sulfonate and carboxylate functional groups were introduced. Its rheological regulation and filtration control performance were systematically investigated in bentonite-based muds and shale gas water-based drilling fluid systems. The main conclusions can be summarised as follows:

(1) Through optimization of synthesis conditions, the optimal preparation parameters were determined to be an SVS/SMAS/MAA molar ratio of 70:20:10, a monomer/bio-PAC mass ratio of 1.4, an APS/bio-PAC mass ratio of 0.50%, and a reaction temperature of 65°C. Structural characterisation confirmed the successful grafting of sulfonate and carboxylate functional groups onto the cellulose backbone. The resulting polymer exhibits favorable thermal stability as well as good environmental compatibility.

(2) In bentonite-based mud systems, PAC-g-(SVS/SMAS/MAA) demonstrates excellent thermal resistance and salt tolerance under freshwater, saturated brine, and mixed-salt conditions, maintaining effective rheological properties and significantly reducing filtration loss after aging at 160°C. In shale gas water-based drilling fluid systems, an optimal dosage of approximately 20 g/L enables a favorable balance between viscosity enhancement and filtration control. Moreover, under high-temperature aging at 160°C–180°C, the drilling fluids treated with PAC-g-(SVS/SMAS/MAA) exhibit markedly superior rheological retention and filtration suppression compared with those treated with commercial HEC and PAC, indicating good engineering adaptability.

(3) Based on the combined analysis of rheological behavior, filtration performance, zeta potential, and filter cake SEM characterization, the performance advantages of PAC-g-(SVS/SMAS/MAA) can be attributed to two primary mechanisms. First, strongly hydrophilic ionic groups enhance hydration and stabilize the spatial network structure, thereby improving the viscosity and structural integrity of the system. Second, the multifunctional architecture promotes particle cementation and pore filling, leading to the formation of dense filter cakes and effective reduction of fluid loss. These characteristics endow PAC-g-(SVS/SMAS/MAA) with promising application potential in high-temperature shale gas water-based drilling fluids.

Acknowledgement: The authors gratefully acknowledge the financial support from the Sichuan Changning Gas Development Co., Ltd. Technical Project (XNS Sichuan Changning JS2025-33).

Funding Statement: This work was supported by the Sichuan Changning Gas Development Co., Ltd. Technical Project (XNS Sichuan Changning JS2025-33).

Author Contributions: The authors confirm contribution to the paper as follows: Conceptualization, Feng Dai and Yinfu Han; methodology, Feng Dai, Jiajun Xie and De Heng; validation, De Heng, Yinfu Han and Yingmin Liu; formal analysis, Jiajun Xie and De Heng; investigation, Yingmin Liu; resources, Yinfu Han; data curation, Shanshan Hou; writing—original draft preparation, Feng Dai and Shanshan Hou; writing—review and editing, Yinfu Han and Shanshan Hou; project administration, Feng Dai and Yinfu Han; funding acquisition, Feng Dai. All authors reviewed and approved the final version of the manuscript.

Availability of Data and Materials: The data that support the findings of this study are available from the corresponding author upon reasonable request.

Ethics Approval: Not applicable.

Conflicts of Interest: The authors declare no conflicts of interest.

References

1. Akpan EU, Enyi GC, Nasr G, Yahaya AA, Ahmadu AA, Saidu B. Water-based drilling fluids for high-temperature applications and water-sensitive and dispersible shale formations. J Petrol Sci Eng. 2019;175(2):1028–38. doi:10.1016/j.petrol.2019.01.002.
2. Du HY, Lv KH, Sun JS, Li MC, Geng Y, Huang XB, et al. Mesoporous SiO_2 nanoparticles with low surface energy and multi-level roughness as shale wellbore stabilizers in oil-based drilling fluid. Petrol Sci. 2025;22(1):384–97. doi:10.1016/j.petsci.2024.12.006.

3. Sun Q, Qiu ZS, Geng T, Zhong HY, Liu W, Tang YL, et al. Application of a hyperbranched amide polymer in high-temperature drilling fluids: inhibiting barite sag and action mechanisms. J Polym Mater. 2025;42(3):757–72. doi:10.32604/jpm.2025.069808.
4. Hu W, Zhang L. Synthesis of hyperbranched polyethyleneimine-propylene oxide-N-isopropylacrylamide (HPEI-co-PO-co-NIPAM) terpolymer as a shale inhibitor. J Polym Mater. 2025;42(4):1159–79. doi:10.32604/jpm.2025.072450.
5. Ahmad HM, Kamal MS, Al-Harthi MA. High molecular weight copolymers as rheology modifier and fluid loss additive for water-based drilling fluids. J Mol Liq. 2018;252(2):133–43. doi:10.1016/j.molliq.2017.12.135.
6. Liu X, Xiao Y, Ding Y. Research progress and prospects of nano plugging agents for shale water-based drilling fluids. ACS Omega. 2025;10(6):5138–47. doi:10.1021/acsomega.4c07942.
7. Wu Y, You F, Hou S. Application of natural materials containing carbohydrate polymers in rheological modification and fluid loss control of water-based drilling fluids: a review. Carbohydr Polym. 2025;348(15):122928. doi:10.1016/j.carbpol.2024.122928.
8. Guo Y, He Y, Du M, Jiang G, Wang Q, Zhang Q. Research and development of eco-friendly high-temperature and salt-resistant filtrate reducers for minimizing drilling fluid loss and environmental pollution. Sep Purif Technol. 2026;392(4):137209. doi:10.1016/j.seppur.2026.137209.
9. Aghdam SB, Moslemizadeh A, Kowsari E, Asghari N. Synthesis and performance evaluation of a novel polymeric fluid loss controller in water-based drilling fluids: high-temperature and high-salinity conditions. J Nat Gas Sci Eng. 2020;83:103576. doi:10.1016/j.jngse.2020.103576.
10. Balding P, Li MC, Wu Q, Volkovinsky R, Russo P. Cellulose nanocrystal-polyelectrolyte hybrids for bentonite water-based drilling fluids. ACS Appl Bio Mater. 2020;3(5):3015–27. doi:10.1021/acsabm.0c00071.
11. Yang P, Li TB, Wu MH, Zhu XW, Sun XQ. Analysis of the effect of polyanionic cellulose on viscosity and filtrate volume in drilling fluid. Mater Res Innov. 2015;19(sup5):S5-12–6. doi:10.1179/1432891715Z.0000000001329.
12. Villada Y, Gallardo F, Erdmann E, Casis N, Olivares L, Estenoz D. Functional characterization on colloidal suspensions containing xanthan gum (XGD) and polyanionic cellulose (PAC) used in drilling fluids for a shale formation. Appl Clay Sci. 2017;149:59–66. doi:10.1016/j.clay.2017.08.020.
13. Khan MA, Li MC, Lv K, Sun J, Liu C, Liu X, et al. Cellulose derivatives as environmentally-friendly additives in water-based drilling fluids: a review. Carbohydr Polym. 2024;342(16):122355. doi:10.1016/j.carbpol.2024.122355.
14. Liu K, Du H, Zheng T, Liu H, Zhang M, Zhang R, et al. Recent advances in cellulose and its derivatives for oilfield applications. Carbohydr Polym. 2021;259(2):117740. doi:10.1016/j.carbpol.2021.117740.
15. Li MC, Wu Q, Song K, Qing Y, Wu Y. Cellulose nanoparticles as modifiers for rheology and fluid loss in bentonite water-based fluids. ACS Appl Mater Interfaces. 2015;7(8):5006–16. doi:10.1021/acsami.5b00498.
16. Li MC, Ren S, Zhang X, Dong L, Lei T, Lee S, et al. Surface-chemistry-tuned cellulose nanocrystals in a bentonite suspension for water-based drilling fluids. ACS Appl Nano Mater. 2018;1(12):7039–51. doi:10.1021/acsanm.8b01830.
17. Khan MA, Lv K, Sun J, Shen H, Zhang Y, Noor AA, et al. Influence of salt and temperature on the rheological and filtration properties of cellulose Nanofiber/bentonite water-based drilling fluids. Geoenergy Sci Eng. 2025;244(9):213524. doi:10.1016/j.geoen.2024.213524.
18. Guo Y, Yang X, Wang R, Zhao M, Wang J, Xie J, et al. Environmentally friendly and temperature resistant water-based drilling fluids with highly inhibitory synthetic nanocellulose polymers for deep sea drilling. Geoenergy Sci Eng. 2024;241(8):213196. doi:10.1016/j.geoen.2024.213196.
19. Khan MA, Lv K, Sun J, Liu F, Shen H, Ding Y, et al. Enhanced filtration performance of cellulose nanofiber/bentonite water-based drilling fluids with temperature- and salt-resistant polymers for extreme conditions. SPE J. 2025;30(9):5327–49. doi:10.2118/228402-pa.
20. Liu F, Jiang G, Peng S, He Y, Wang J. Amphoteric polymer as an anti-calcium contamination fluid-loss additive in water-based drilling fluids. Energy Fuels. 2016;30(9):7221–8. doi:10.1021/acs.energyfuels.6b01567.
21. Liu X, Yuan Z, Wang A, Wang C, Qu J, Chen B, et al. Cellulose nanofibril-polymer hybrids for protecting drilling fluid at high salinity and high temperature. Carbohydr Polym. 2020;229(3):115465. doi:10.1016/j.carbpol.2019.115465.

22. Balaga DK, Kulkarni SD. A review of synthetic polymers as filtration control additives for water-based drilling fluids for high-temperature applications. J Petrol Sci Eng. 2022;215(30):110712. doi:10.1016/j.petrol.2022.110712.
23. Jia X, Zhao X, Chen B, Egwu SB, Huang Z. Polyanionic cellulose/hydrophilic monomer copolymer grafted silica nanocomposites as HTHP drilling fluid-loss control agent for water-based drilling fluids. Appl Surf Sci. 2022;578:152089. doi:10.1016/j.apsusc.2021.152089.
24. Cao J, Meng L, Yang Y, Zhu Y, Wang X, Yao C, et al. Novel acrylamide/2-acrylamide-2-methylpropanesulfonic acid/4-vinylpyridine terpolymer as an anti-calcium contamination fluid-loss additive for water-based drilling fluids. Energy Fuels. 2017;31(11):11963–70. doi:10.1021/acs.energyfuels.7b02354.
25. Li J, Ji YX, Ni XX, Lv KH, Huang XB, Sun JS. A micro-crosslinked amphoteric hydrophobic association copolymer as high temperature- and salt-resistance fluid loss reducer for water-based drilling fluids. Petrol Sci. 2024;21(3):1980–91. doi:10.1016/j.petsci.2024.01.021.
26. Wang G, Jiang G, Yang J, Yang L, Li X, He Y, et al. NovelN, N-dimethylacrylamidecopolymer containing multiple rigid comonomers as a filtrate reducer inwater-baseddrilling fluids and mechanism study. J Appl Polym Sci. 2021;138(39):51001. doi:10.1002/app.51001.
27. Liu J, Xia Y, Ma J. Development and application of eco-friendly micro-nano filtrate reducers and high-performance water-based drilling fluids. Acadlore Trans Geosci. 2024;3(2):98–105. doi:10.56578/atg030204.
28. Li A, Gao S, Zhang G, Zeng Y, Hu Y, Zhai R, et al. A review in polymers for fluid loss control in drilling operations. Macromol Chem Phys. 2024;225(8):2300390. doi:10.1002/macp.202300390.
29. Zhao Y, Zhao H, Shao S, Wen G. Scale inhibition mechanism of itaconic acid-sodium methacrylate sulfonate on calcite: quantum chemical calculation and molecular dynamics simulation. J Mol Liq. 2024;411:125672. doi:10.1016/j.molliq.2024.125672.
30. Wang C, Jin L, Liu X, Zhang N, Liu H, Ding W. Preparation and evaluation of high-temperature filtrate reducer for solid-free water-based drilling fluid. Polym Eng Sci. 2022;62(8):2411–8. doi:10.1002/pen.26015.
31. Chung YT, Huang CI. Ion condensation behavior and dynamics of water molecules surrounding the sodium poly(methacrylic acid) chain in water: a molecular dynamics study. J Chem Phys. 2012;136(12):124903. doi:10.1063/1.3697477.
32. Haleem N, Arshad M, Shahid M, Tahir MA. Synthesis of carboxymethyl cellulose from waste of cotton ginning industry. Carbohydr Polym. 2014;113(12):249–55. doi:10.1016/j.carbpol.2014.07.023.
33. Shi S, Zhang M, Ling C, Hou W, Yan Z. Extraction and characterization of microcrystalline cellulose from waste cotton fabrics via hydrothermal method. Waste Manag. 2018;82:139–46. doi:10.1016/j.wasman.2018.10.023.
34. Wang C, Su J, Liu T, Ge S, Liew RK, Zhang H, et al. A sustainable strategy to transform cotton waste into renewable cellulose fiber self-reinforcing composite paper. J Clean Prod. 2023;429(2):139567. doi:10.1016/j.jclepro.2023.139567.
35. Wang Z, Yao Z, Zhou J, Zhang Y. Reuse of waste cotton cloth for the extraction of cellulose nanocrystals. Carbohydr Polym. 2017;157(3):945–52. doi:10.1016/j.carbpol.2016.10.044.
36. Wu Y, You F, Hou S, Zhou S. Study of a novel cross linked graft copolymer starch in water-based drilling fluid. Mater Res Express. 2023;10(5):055501. doi:10.1088/2053-1591/acd227.
37. Gao X, Zhong HY, Zhang XB, Chen AL, Qiu ZS, Huang WA. Application of sustainable basil seed as an eco-friendly multifunctional additive for water-based drilling fluids. Petrol Sci. 2021;18(4):1163–81. doi:10.1016/j.petsci.2021.05.005.
38. Chang X, Sun J, Xu Z, Zhang F, Wang J, Lv K, et al. A novel nano-lignin-based amphoteric copolymer as fluid-loss reducer in water-based drilling fluids. Colloids Surf A Physicochem Eng Aspects. 2019;583:123979. doi:10.1016/j.colsurfa.2019.123979.
39. Akpan EU, Enyi GC, Nasr GG. Enhancing the performance of xanthan gum in water-based mud systems using an environmentally friendly biopolymer. J Petrol Explor Prod Technol. 2020;10(5):1933–48. doi:10.1007/s13202-020-00837-0.
40. Wei Z, Wang M, Li Y, An Y, Li K, Bo K, et al. Sodium alginate as an eco-friendly rheology modifier and salt-tolerant fluid loss additive in water-based drilling fluids. RSC Adv. 2022;12(46):29852–64. doi:10.1039/d2ra04448j.

41. Li D, Bai Y, Liu L, Su N, Hu J, Wang C, et al. High-temperature and high-salt water-based drilling fluid loss reducing agent: synthesis, performance evaluation and mechanism. Colloids Surf A Physicochem Eng Aspects. 2026;730:139025. doi:10.1016/j.colsurfa.2025.139025.
42. Mao H, Qiu Z, Shen Z, Huang W. Hydrophobic associated polymer based silica nanoparticles composite with core-shell structure as a filtrate reducer for drilling fluid at utra-high temperature. J Petrol Sci Eng. 2015;129:1–14. doi:10.1016/j.petrol.2015.03.003.
43. Yang X, Shang Z, Liu H, Cai J, Jiang G. Environmental-friendly salt water mud with nano-SiO_2 in horizontal drilling for shale gas. J Petrol Sci Eng. 2017;156:408–18. doi:10.1016/j.petrol.2017.06.022.